**Live-cell imaging and CLEM reveal the existence of ACTN4-dependent ruffle-edge lamellipodia acting as a novel mode of cell migration**

Haruka Morishita[1], Katsuhisa Kawai[1], Youhei Egami[1], Kazufumi Honda[2], Nobukazu Araki[1*]

[1]Department of Histology and Cell Biology, School of Medicine, Kagawa University
Miki, Kagawa 761-0793, Japan
[2]Department of Bioregulation, Graduate of Medicine, Nippon Medical School, Sendagi, Bunkyo-ku, Tokyo 113-8602, Japan

*Corresponding author (araki.nobukazu@kagawa-u.ac.jp)
Department of Histology and Cell Biology, School of Medicine, Kagawa University,
Miki, Kagawa-761-0793, Japan

**Summary**

α-Actinin-4 (ACTN4) expression levels are correlated with the invasive and metastatic potential of cancer cells; however, the underlying mechanism remains unclear. Here, we identified ACTN4-localized ruffle-edge lamellipodia using live-cell imaging and correlative light and electron microscopy (CLEM). BSC-1 cells expressing EGFP-ACTN4 showed that ACTN4 was most abundant in the leading edges of lamellipodia, although it was also present in stress fibers and focal adhesions. ACTN4 localization in lamellipodia was markedly diminished by phosphoinositide 3-kinase inhibition, whereas its localization in stress fibers and focal adhesions was unaffected. Furthermore, overexpression of ACTN4, but not ACTN1, promoted lamellipodial formation. Live-cell analysis demonstrated that ACTN4-enriched lamellipodia are highly dynamic and associated with cell migration. CLEM revealed that ACTN4-enriched lamellipodia exhibit a characteristic morphology of multilayered ruffle-edges that differs from canonical flat lamellipodia. Similar ruffle-edge lamellipodia were observed in A549 and MBA-MD-231 invasive cancer cells. ACTN4 knockdown suppressed the formation of ruffle-edge lamellipodia and cell migration during wound healing in A549 monolayer cultures. Additionally, membrane-type 1 metalloproteinase was observed in the membrane ruffles, suggesting that ruffle-edge lamellipodia have the ability to degrade the extracellular matrix and may contribute to active cell migration/invasion in certain cancer cell types.

**Keywords:** ACTN4, lamellipodia, PI3K, cell migration, live-cell imaging, CLEM

**Abbreviations:** ACTN4, actinin-4; Arp2/3, Actin-related protein 2/3;
EGFP, enhanced green fluorescent protein; CLEM, correlative light-electron microscopy; PH domain, pleckstrin homology domain; PI3K, phosphoinositide 3-kinase; PI(4,5)$P_2$, phosphatidylinositol 4,5-bisphosphate; PI(3,4,5)$P_3$, phosphatidylinositol 3,4,5-triphosphate; PMA, phorbol 12-myristate 13-acetate; N-WASP, neuronal Wiskott-Aldrich syndrome protein; WAVE, WASP family verprolin-homologous protein.

## Introduction

Cell migration is essential for many physiological and pathological processes, such as embryonic development, wound healing, inflammation, and cancer cell invasion. Although diverse modes of cell migration, including membrane blebbing and cytoplasmic streaming, are used for various purposes by different cell types [1], the migration mechanism through lamellipodial protrusions appears to be the primary one in many cases. In general, lamellipodia are defined as thin, sheet-like cell protrusions that constitute the actin cytoskeleton-based motile apparatus, which is indispensable for promoting the movement of migrating cells [2]. Cell migration is established by progressive extension of lamellipodia using basal cell adhesion as a scaffold and retraction of the posterior tail of the cell [3,4]. The extension of lamellipodia is initiated by the formation of a network of branched actin filaments (F-actin) through the Arp2/3 complex, which is activated by nucleation promoting factors such as the WAVE regulatory complex (WRC)[5–8]. The Rho-family GTPase Rac1 is a major switch molecule that regulates lamellipodial formation [9]. GTP-bound Rac1, which is targeted to the plasma membrane, activates the WRC-Arp2/3-F-actin nucleation axis, thereby facilitating membrane protrusion [10,11]. Dynamic changes in the actin cytoskeleton architecture inside the formed lamellipodia are driven by a variety of actin-binding proteins, including lamellipodin [12], cortactin [13], cofilin [14], α-actinin, and myosins [15]. These proteins are known to be regulated by membrane phospholipids such as phosphatidylinositol 4,5-bisphosphate ($PI(4,5)P_2$) and phosphatidylinositol 3,4,5-triphosphate ($PI(3,4,5)P_3$) [16]. $PI(3,4,5)P_3$ is produced from $PI(4,5)P_2$ by class I phosphoinositide 3-kinase (PI3K) and is concentrated in projecting lamellipodia, as well as GTP-bound Rac1 [10,17–19]. When lamellipodia detach from the substratum and roll up, their structure and motion are termed membrane ruffles and ruffling, respectively. Membrane ruffles arising from the cell periphery move centripetally to the dorsal cell surface. Although the term ‘membrane ruffles’ is commonly used for various structures, including peripheral ruffles [18], circular ruffles (macropinocytic cups) [20,21], and dorsal circular ruffles [22], the morphology and functions of membrane ruffles may vary considerably depending on the cell type and specific circumstances.

α-Actinin (ACTN) is an actin-binding protein, and its two isoforms, ACTN1 and ACTN4, exist in non-muscle cells. ACTN1 primarily localizes to focal adhesion plaques and anchors F-actin stress fibers to the plasma membrane with proteins, including talin, vinculin, and integrin [23,24]. In 1998, ACTN4 was cloned as a new isoform associated with cancer cell invasion [25]. Although ACTN1 and ACTN4 are highly homologous in their nucleotide and amino acid sequences, ACTN4 is presumed to be preferentially involved in more dynamic cellular structures, including lamellipodia and membrane ruffles [21,25–27]. In recent years, *in vitro* and *in vivo* studies have demonstrated a correlation between increased ACTN4 expression and several advanced cancers including oral, breast, colorectal, and pancreatic cancers [28–30]. Several lines of evidence have implicated ACTN4

in the invasion and metastasis of cancer cells [29,31–33]. Evidence now describes ACTN4 as a useful biomarker indicative of cancer progression and prognosis, and a potential therapeutic target in patients with various cancers [29,32]. However, the precise role of ACTN4 in lamellipodial formation associated with cell migration remains to be elucidated.

Recently, we found highly motile lamellipodia with DENND1B-positive structures at the bottom, which were most conspicuously observed in BSC-1 cells [37]. In exploring key molecules characterizing the lamellipodia, we found that ACTN4 is abundantly observed in the lamellipodia. In this study, live-cell imaging and correlative light-electron microscopy (CLEM) demonstrate that ACTN4-enriched lamellipodia exhibit special morphological and functional phenotypes of cell migration and invasion. We further show that the formation of a special form of lamellipodia is highly dependent on PI3K activity. Importantly, ACTN4 knockdown inhibits lamellipodia formation and cell migration. Since the leading edge of lamellipodia shows extracellular matrix degradation activity, the formation of ACTN4-enriched lamellipodia may act as a novel mode of cell migration and invasion. Our findings provide new insights into why ACTN4 is associated with enhanced cell migration and could be linked to the progression of certain types of cancer.

## Materials and Methods

### *Reagents and Plasmids*

Full-length cDNA encoding human ACTN4 was amplified by PCR. The fragment was cloned into the pEGFP vector. pmCherry-Lifeact was constructed by cloning the synthesized cDNA fragment of Lifeact into pmCherry vector. pEGFP-ACTN1 (Addgene #11908) was obtained from Dr. Carol Otey (UNC-Chapel Hill) and pTriEx/mCherry-PA-Rac1 (Addgene #22024) was obtained from Dr. Klaus Hahn (UNC-Chapel Hill). pmCitrine-Rac1, pmCitrine-Rac1Q61L, pmCitrine-Rac1T17N, pCFP-membrane, pmCitrine-Akt-PH, and pYFP-Btk-PH domains were gifts from Dr. Joel A. Swanson (University of Michigan). The pmCherry-Akt-PH domain and pmCherry-membrane were generated by replacing mCitrine or CFP cDNA with mCherry cDNA. Other reagents were purchased from FUJIFILM Chemicals (Osaka, Japan) or Nacalai Tesque (Kyoto, Japan), unless otherwise indicated.

### *Cell culture, and transfection*

BSC-1 cells, epithelial cells of African green monkey kidney origin, were obtained from the JCRB Cell Bank (Osaka, Japan). HeLa, MDCK-II, B16, A549, A431, and RAW264 cells were obtained from the Riken Cell Bank (Tsukuba, Japan). MDA-MB-231 cells were obtained from the ATCC (Manassas, VA). The cells were cultured in Dulbecco's modified Eagle's medium (DMEM) supplemented with 10% heat-inactivated fetal bovine serum (FBS) and antibiotics (penicillin and streptomycin) at 37°C in a humidified atmosphere containing 5% $CO_2$. Cells were transfected with plasmids using the Neon Transfection System (Life Technologies, Carlsbad, CA), according to the manufacturer’s protocols. The cells were seeded onto 13- or 25-mm circular coverslips in culture dishes containing the culture media. The cells were used for experiments 12–24 h after transfection.

### *ACTN4 siRNA knockdown and wound healing assay*

ACTN4 knockdown experiments were performed using Stealth Select RNAi (Thermo Fisher Scientific). A549 cells were transfected with small interfering RNA (siRNA) targeting human ACTN4 (#1 HSS100124, #2 HSS100125, #3 HSS188682), human ACTN1 (HSS100130), or negative control siRNA (Med GC Duplex#3) using Lipofectamine RNAiMAX (Thermo Fisher Scientific) according to the manufacturer's instructions. The cells were subjected to experiments 48–72 h after transfection. The knockdown effects of ACTN1 and ACTN4 siRNAs were confirmed by immunoblotting and immunofluorescence assays. We quantified the knockdown efficiency by measuring the fluorescence intensity of ACTN4 immunofluorescence staining in A549 cells using the MetaMorph imaging system. Each group of cells was immunostained and imaged under identical conditions. The fluorescence intensity relative to that of the negative control siRNA-treated cells was calculated after background subtraction.

To observe migrating cells, a confluent monolayer of A459 cells on coverslips was scratched with a 200 μL pipette tip. After 5–24 h, the cells that migrated from the edge of the artificial wound were observed. Using ACTN4 knockdown A549 cells, a wound healing assay was performed to

determine the cell migration capacity by measuring the changes in wound width by subtracting the width of the wounds at 5 h from that at 0 h after scraping.

***Immunoblotting***

Total protein lysates were prepared with a lysis buffer consisting of 50 mM Tris-HCl (pH 7.5), 150 mM NaCl, 1% Triton X-100, 0.5% sodium deoxycholate, 0.1% sodium dodecyl sulfate (SDS), 0.1% CHAPS, and protease inhibitor cocktail (Nacalai Tesque, Kyoto, Japan). Equal amounts of protein were denatured and reduced with sample buffer containing 1% SDS and 2.5% 2-mercaptoethanol. The samples were subjected to 10% SDS-PAGE and transferred to polyvinylidene difluoride membranes (Millipore, Bedford, MA, USA). The membranes were immunoreacted with anti-ACTN4 mouse monoclonal IgG (Abnova, clone 13G9, dilution 1:10000), or anti-ACTN1 rabbit polyclonal IgG (Abcepta, clone RB21901, 1:1000). Anti-GAPDH mouse monoclonal antibody (Ambion, clone 6C5, 1:10000) was used to verify equal amounts of total protein loading. After washing, the membranes were incubated with HRP-conjugated anti-rabbit IgG or anti-mouse IgG secondary antibodies and developed using the ECL Prime Western Blotting Detection System (Cytiva, Tokyo, Japan).

***Live-cell imaging***

For live-cell imaging, cells were cultured on 25-mm circular coverslips. Before imaging, the culture medium was replaced with Ringer's buffer (RB) consisting of 155 mM NaCl, 5 mM KCl, 1 mM $MgCl_2$, 2 mM $Na_2HPO_4$, 10 mM glucose, 10 mM HEPES and 0.5 mg/ml bovine serum albumin (BSA) at pH 7.2. The 25-mm circular coverslip was assembled in an RB-filled chamber (Attofluor, #A7816, Molecular Probes) and placed on a 37°C thermo-controlled stage in Leica DMI6000B inverted microscope (Leica Microsystems, Wetzlar, Germany). Live-cell images were acquired with an oil-immersion 100× objective lens (HC PL Fluotar PH3, NA=1.32 or HCX PL Apo, NA=1.4) using an Orca Flash 4.2 sCMOS camera (Hamamatsu Photonics, Shizuoka, Japan) under the control of the MetaMorph Imaging software (Molecular Devices). Kymographs were generated using MetaMorph software by taking 1-pixel wide rectangular regions in the direction of lamellipodial extension.

***Optogenetics of photoactivatable Rac1 under the fluorescence microscope***

Cells transfected with pTriEx/mCherry-PA-Rac1Q61L and pEGFP-ACTN4 were cultured on 25 mm circular coverslips for 16-24 h. The coverslips were subjected to live-cell imaging as described above. Optogenetic control of photoactivatable (PA)-Rac1 under the Leica DMI6000B microscope was achieved using a journal (macro-program) of MetaMorph software, which automates the acquisition of time-lapse images and photoactivation during the image acquisition interval [34]. Because the light oxygen voltage 2 (LOV2) domain of PA-Rac1 is a photosensor for blue light (360–500 nm), we activated PA-Rac1 by illuminating the cells through a cyan fluorescent protein (CFP) excitation filter (Chroma ET436/24 nm). When illuminated with blue light, the LOV2 domain

undergoes a conformational change that enables downstream effector binding to Rac1, indicating that the cells exhibit a constitutively active Rac1 phenotype [35,36].

***Immunofluorescence microscopy***

BSC-1 cells on coverslips were fixed with 4% paraformaldehyde (PFA) in 0.1M phosphate buffer (pH 7.4) containing 6% sucrose for 30 min at room temperature. After rinsing with phosphate-buffered saline (PBS), the cells were permeabilized with 0.25% Triton X-100/PBS and blocked with 1% BSA/0.5% gelatin/PBS for 10 min each. The cells were then incubated with rabbit polyclonal anti-ACTN4 antibody (dilution 1:100)[25] or mouse monoclonal anti-ACTN4 antibody (Abnova, Clone 13G9, dilution 1:300) for 60 min, followed by incubation with a secondary antibody conjugated with Alexa Fluor 488 or 594 (Molecular Probes, 1:1000). An anti-vinculin mouse monoclonal antibody (V9264; Sigma-Aldrich, 1:200) was used as a focal contact marker. Membrane-type 1 matrix metalloproteinase (MT1-MMP; also known as MMP14) was detected in A549 cells fixed with 1% paraformaldehyde for 5 min using an anti-MT1-MMP rabbit monoclonal antibody (1:100 dilution, EP1264Y, Abcam). F-actin was stained with Alexa Fluor 350- or 568-conjugated phalloidin (Molecular Probes) or Acti-stain 670 phalloidin (Cytoskeleton Inc.). Nuclear staining was performed using 4',6-diamidino-2-phenylindole (DAPI) solution (1 μg/ml in PBS).

The specimens were mounted onto glass slides and examined under a confocal microscope (LSM710, Carl Zeiss, Oberkochen, Germany) or an epifluorescence microscope (Leica DMI6000B). Some specimens were observed by a confocal-based super-resolution microscope (Nikon AX with NSPARC detector) using a plan apo 60× NA=1.42 objective lens.

***Correlative light-electron microscopy (CLEM)***

Cells transfected with pEGFP-ACTN4 were cultured on grided coverslips in 35 mm dishes and fixed with 2% glutaraldehyde in 0.1M phosphate buffer (pH 7.4) for 30 min. Coverslips in a PBS-filled dish were observed under a Zeiss LSM710 confocal laser microscope using a 40x Plan Apochromat water immersion objective lens (N.A. 1.0). EGFP-ACTN4 fluorescence and DIC images were obtained using ZEN software. The coverslips were then post-fixed with 1% $OsO_4$ and processed for scanning electron microscopy as previously described [37]. Critical point-dried specimens were coated with osmium using an osmium plasma coater (OPC40, Nippon Laser & Electronics) and observed with a field-emission scanning electron microscope (EM) (Hitachi S900) at 6 kV. The same cell was photographed through the confocal laser microscope was searched and photographed using scanning EM. Scanning EM and confocal fluorescence images were overlaid using Adobe Photoshop. Similarly, cells immunostained with anti-ACTN4 were processed to scanning EM after fluorescence microscopy for subjecting to CLEM.

***Fluorescein gelatin degradation assay***

Sterilized coverslips were coated with 0.1 mg/ml poly-L-lysine for 20 min, washed with PBS, and fixed with 0.5% glutaraldehyde for 10 min. After three washes with PBS, the coverslips were

inverted on a 40-μl drop of 0.2% fluorescein (FITC)-labeled gelatin (Thermo Fisher Scientific) in 2% sucrose in PBS and incubated for 10 min. After washing with PBS, free aldehyde groups were quenched with 1 mg/ml sodium borohydride in PBS for 5 min, washed three times in PBS, and incubated with 1 ml of complete medium for 30 min. Cells were plated on fluorescent gelatin-coated coverslips, incubated for 30-60 min, and then fixed with 4% paraformaldehyde for 30 min. The samples were processed for staining with anti-ACTN4 monoclonal antibody and ActiStain 670 phalloidin. The coverslips were imaged using a Nikon AX confocal microscope.

***Statistical analysis***

For quantitative analysis, data were obtained from at least three independent measurements and expressed as the mean ± standard error of the mean (SEM) or standard deviation (SD). Statistical significance was calculated using a two-tailed Student's *t*-test or one-way analysis of variance (ANOVA), followed by Tukey's test. Differences were considered statistically significant at $P < 0.05$.

## Results

### *Localization of endogenous ACTN4 and its PI3K dependency in BSC-1 cells*

First, we examined the localization of endogenous ACTN4 in control BSC-1 cells by anti-ACTN4 immunofluorescence and phalloidin staining for F-actin. Confocal microscopy revealed that ACTN4 is abundantly localized in F-actin-based structures, including lamellipodia, actin stress fibers, and focal adhesions (Fig. 1A). However, the localization pattern of ACTN4 varies considerably among cells. Typically, BSC-1 cells with ACTN4-enriched lamellipodia had fewer stress fibers. In contrast, cells without lamellipodia showed ACTN4-positive stress fibers and focal adhesions. Based on the ACTN4 localization pattern, we classified the cells into three types, examples of which are shown in Fig.1A: (i) lamellipodia type (L-type), in which ACTN4 predominantly localizes in lamellipodia (Fig.1A, inset a); (ii) intermediate type (I-type), in which ACTN4 moderately localizes in both lamellipodia and stress fibers/focal adhesions (Fig. 1A, inset b); and (iii) stress fiber type (SF-type), in which ACTN4 predominantly localizes in stress fibers/focal adhesions (Fig. 1A, inset c). We then calculated the percentage of each type in BSC-1 cells by counting the number of each type in > 60 cells/coverslip (total 6 coverslips from three independent experiments) under fluorescence microscopy of anti-ACTN4 immunoreaction and phalloidin staining. Among control BSC-1 cells, L-type cells were 18.13±3.22% (n=6 coverslips), SF-type cells were 37.03±4.01% (n=6 coverslips), and I-type cells were 44.18±4.80% (n=6 coverslips) (Fig. 1C).

Phosphoinositides, such as PI(4,5)$P_2$ and PI(3,4,5)$P_3$, are known to be crucial regulators of actin cytoskeleton organization and membrane trafficking [16,38,39]. Fraley et al. (2003) reported that PI(3,4,5)$P_3$ binds to the N-terminal calponin homology domain of actinin and downregulates its actin-bundling ability [40]. Therefore, we examined the effect of LY294002, a PI3K inhibitor that inhibits the production of PI(3,4,5)$P_3$ from PI(4,5)$P_2$, on the localization of ACTN4 in BSC-1 cells. ACTN4-enriched lamellipodia were scarcely observed in LY294002-treated cells. The localization of ACTN4 in stress fibers and focal adhesions was not significantly affected by treatment with the PI3K inhibitor LY294002 (Fig. 1B). Counting the number of cells with ACTN4-enriched lamellipodia revealed that LY294002 treatment significantly reduced the proportion of L-type cells instead of increasing the number of SF-type cells (Fig. 1C).

### *Overexpression of ACTN4, but not ACTN1, increases lamellipodia formation*

Next, we examined the localization of exogenously overexpressed ACTN4 or ACTN1 in BSC-1 cells by transfecting pEGFP-ACTN4 or pEGFP-ACTN1 together with pmCherry-Lifeact. Although both EGFP-ACTN1 and EGFP-ACTN4 were observed in lamellipodia, stress fibers, and focal adhesions, they showed distinct distribution quantities among the actin-based structures (Fig.2A-D, Supplementary Figs. S1-3). In EGFP-ACTN4-overexpressing cells, ACTN4 was highly abundant in lamellipodia (Fig.2A, Supplementary Fig. S1). In contrast, ACTN1 was enriched in stress fibers and

focal adhesions at both ends of stress fibers in EGFP-ACTN1-overexpressing cells. ACTN1-enriched lamellipodia were observed less frequently (Fig.1D, Supplementary Fig. S2). To examine the impact of ACTNs overexpression, we calculated the percentage of each type of cell overexpressing EGFP-ACTN4 or EGFP- ACTN1 by counting the number of each type of cell in > 60 cells/coverslip (total 6 coverslips from three independent experiments) under phase-contrast and fluorescence microscopy of mCherry-Lifeact and EGFP-ACTNs. Among the ACTN4-overexpressing cells, L-type cells were ~50%, which was more than double that in control BSC-1 cells, SF-type was ~30%, and I-type was ~20%. In contrast, among the ACTN1-overexpressing cells, L-type accounted for ~10%, SF-type for ~70%, and I-type for ~20% (Fig.2E). Thus, the number of L-type cells was significantly increased by ACTN4 overexpression compared to ACTN1 overexpression. These results suggest that ACTN4 overexpression may facilitate lamellipodia formation, whereas ACTN1 overexpression may have a higher propensity to form stress fibers and focal adhesions in BSC-1 cells. Compared with the data from control BSC-1 cells (Fig.1E), overexpression of ACTN4 appears to have a promoting effect on lamellipodia formation; in contrast, ACTN1 overexpression may suppress it.

***PI3K activity is indispensable for ACTN4 localization to lamellipodia, but not to stress fibers or focal adhesions***

Live-cell imaging and high-resolution confocal microscopy of BSC-1 cells expressing EGFP-ACTN4 showed that EGFP-ACTN4 in lamellipodia was markedly diminished after the addition of the PI3K inhibitor, whereas ACTN4 localization in stress fibers and focal adhesions was not significantly affected (Fig.2F, Supplementary Fig. S3, Movie 1). Quantitation of ACTN4 localization types revealed that the percentage of the L-type was drastically reduced to only 2% by PI3K inhibition, and instead the SF-type increased to ~70% (Fig.2E). These findings suggest that PI3K activity is indispensable for ACTN4 localization in lamellipodia, whereas that in stress fibers and focal adhesions may not require PI3K activity.

As ACTN1 was predominantly localized in stress fibers and focal adhesions in control BSC-1 cells, the localization of ACTN1 was significantly altered by PI3K inhibition (Supplementary Fig. S2). Therefore, ACTN1-overexpressing cells showed fewer changes in the percentage of each type compared to ACTN4-overexpressing cells. ACTN1-overexpressing cells originally exhibited fewer L-type cells; however, the percentage of L-type cells significantly decreased after PI3K inhibition (Fig. 2E). These results indicate that overexpression of ACTN4, but not ACTN1, may promote lamellipodia formation in a PI3K-dependent manner.

To clarify the relationship between PI3K and ACTN4 in live cells, we monitored the major products of class I PI3K, PI(3,4,5)$P_3$/PI(3,4)$P_2$, by co-expressing mCherry-Akt pleckstrin homology domain (Akt-PH) and EGFP-ACTN4. As expected, mCherry-Akt-PH signal levels were particularly high in the region of extending lamellipodia enriched with EGFP-ACTN4 (Fig. 3). However,

mCherry-Akt-PH signals were scarcely observed in stress fibers or focal adhesions. When LY294002 was applied to the cells, mCherry-Akt-PH signals in ACTN4-enriched lamellipodia immediately disappeared. Almost simultaneously, EGFP-ACTN4 expression was diminished in the lamellipodia (Fig. 3), whereas EGFP-ACTN4 remained in the stress fibers and focal adhesions (Fig. 3A, Supplementary Fig. S3). A decrease in PI(3,4,5)$P_3$/PI(3,4)$P_2$ concentrations in the membrane of lamellipodia was verified by ratio imaging of mCitrine-Akt-PH/mCherry-membrane (Supplementary Fig. S4A). Using the YFP-Btk-PH probe, which binds only to PI (3, 4, 5) P3, we obtained results similar to those obtained with the Akt-PH probe (Supplementary Fig. S4B, Movie 2). These observations suggest that PI(3,4,5)$P_3$ may be an important factor in ACTN4 localization to lamellipodia.

***ACTN4-enriched lamellipodia are highly dynamic and invasive structures***

To characterize the dynamics of ACTN4-enriched lamellipodia, time-lapse movies of live BSC-1 cells expressing EGFP-ACTN4 were created. A movie of EGFP-ACTN4-expressing BSC-1 cells showed that extending lamellipodia were rich in ACTN4, whereas retracting or static lamellipodia-like protrusions were ACTN4-modest (Fig. 4A, Movie 3). The moving speed of the ACTN4-enriched lamellipodia was much faster than that of ACTN4-modest protrusions. Therefore, the dynamics of lamellipodia were assessed by kymograph analysis using MetaMorph software (Fig. 4B). ACTN4-enriched lamellipodia always extended forward at an average speed of 0.37±0.15 µm/min (n=15 lamellipodia collected from 3 independent experiments), whereas ACTN4-modest flat protrusions moved with repeated extension and retraction. Because the leading edge of flat protrusions fluctuated with almost equal amplitude of extension and retraction, only a small net advance (0.07±0.04 µm/min, n=15, collected from 3 independent experiments) was observed. It is also notable that ACTN4-enriched lamellipodia have wavy structures at their leading edges. These wavy structures were recognized as phase-dark structures, similar to membrane ruffles, by phase-contrast microscopy. However, compared with canonical membrane ruffles observed in macrophage colony-stimulating factor (m-CSF)-stimulated macrophages and epidermal growth factor (EGF)-stimulated A431 cells, ACTN4-enriched ruffle-like structures of lamellipodia were smaller and tightly stacked at the leading edge (Movie 4). It has previously been shown that membrane ruffling in macrophages and A431 cells is resistant to PI3K inhibition, although the process of membrane ruffle closure to macropinosomes is PI3K-dependent [20,41]. Therefore, the ruffle-like structures of the lamellipodial leading edges may be somewhat different from those of the canonical membrane ruffles.

The long-term movie over several hours showed that BSC-1 cells expressing EGFP-ACTN4 dynamically migrate upon extending lamellipodia with phase-dark wavy leading edges. However, when lamellipodia were static or retracting, wavy structures were absent from the leading edges (Movie 5). Thus, the wavy edge structures of the lamellipodial leading edges may be hallmarks of

progressive lamellipodia. Taken together, these results suggest that ACTN4 plays a role in the ability of cells to form highly dynamic lamellipodia through recruitment to the PI(3,4,5)$P_3$-enriched plasma membrane.

***CLEM revealed that ACTN4-enriched lamellipodia have multilayered membrane folds at their leading edges***

To clarify the ultrastructural features of phase-dark wavy-edge lamellipodia observed under phase-contrast microscopy, we performed CLEM on BSC-1 cells expressing EGFP-ACTN4. First, BSC-1 cells transfected with pEGFP-ACTN4 were cultured on gridded glass coverslips in 35 mm dishes and fixed with 2% glutaraldehyde in a buffer. After washing with PBS, the specimens were observed and photographed with a Zeiss LSM710 confocal microscope using a Plan-Apochromat 40× water-immersion objective lens to identify the precise location of cells expressing EGFP-ACTN4. We then processed the specimen coverslips for scanning EM and observed the same area under the scanning EM. Scanning EM showed that ACTN4-enriched lamellipodia have a characteristic ultrastructure; the leading edges of ACTN4-enriched lamellipodia have multilayered membrane folds. Consistent with phase-contrast microscopy results, membrane folds at the lamellipodial leading edges, where ACTN4 was particularly concentrated, were shorter but more densely present than membrane ruffles in RAW macrophages and A431 cells (Fig. 5, Supplementary Fig. S5). Consequently, it can be asserted that multilayered membrane folds at the lamellipodial leading edges are strictly distinct from the simple membrane ruffles observed in other cell types, although they can be broadly considered small ruffles. Thus, we found that ACTN4-enriched lamellipodia in BSC-1 cells possess a unique morphological feature characterized by multilayered ruffles at the leading edge. Based on this characteristic, we hereafter refer to them as “ruffle edge lamellipodia” to distinguish them from the conventional flat lamellipodia.

***Formation of ACTN4-enriched ruffle-edges may require Rac1activation/deactivation cycling***

It is well-known that Rac1 activation is required for canonical lamellipodial formation [9,42,43]. However, the involvement of Rac1 activity in the formation of ACTN4-enriched ruffle-edge lamellipodia remains unknown. Therefore, we examined the effect of Rac1 mutant overexpression on ACTN4-enriched lamellipodia. BSC-1 cells were transfected with pmCitrine-fused wild-type Rac1 (Rac1 WT), a constitutively active GTP-lock mutant (Rac1 Q61L), or a dominant-negative GDP-lock mutant (Rac1 T17N). Following fixation, ACTN4 was detected by immunostaining with an anti-ACTN4 antibody, followed by incubation with an Alexa Fluor 594-labeled secondary antibody. In cells expressing Rac1 WT, ACTN4-enriched lamellipodia were notable. In contrast, constitutively active Rac1 Q61L expressing cells exhibited ACTN4-modest flat leading-edge lamellipodia along the outer perimeter. In Rac1 T17N expressing cells, both types of lamellipodia were rarely observed (Fig. 6A). To confirm the involvement of Rac1 activity in the formation of ruffle-edge lamellipodia, we applied optogenetic control of PA-Rac1 in live BSC-1 cells co-

expressing EGFP-Rac1 and mCherry-PA-Rac1. In the dark, cells expressing PA-Rac1 had ACTN4-enriched ruffle-edge lamellipodia, probably owing to endogenous wild-type Rac1 activity. Continuous photoactivation of PA-Rac1 by blue light illumination for several minutes changed the lamellipodia phenotype from ACTN4-enriched ruffle-edge lamellipodia to ACTN4-modest flat-edge lamellipodia, as observed in Rac1Q61L-expressing cells (Fig. 6B, Movie 6). These results indicate that Rac1 activation-deactivation cycling may be indispensable for ruffle-edge lamellipodia, whereas Rac1 activation is sufficient for the extension of canonical flat lamellipodia.

***The ruffle edge lamellipodia are frequently observed in highly invasive cancer cells***

Finally, we investigated whether the presence of ruffle-edge lamellipodia is cell type-specific using several representative cell lines: HeLa, MDCK-II, B16, A549, and MDA-MB-231 cells (Fig. 7, Supplementary Figs. S6-9). In HeLa cells, lamellipodia were rarely observed. ACTN4 was predominantly localized to stress fibers and focal adhesions. Although MDCK-II cells occasionally exhibited lamellipodia, their leading edges were not enriched with ACTN4. B16 mouse melanoma cells frequently exhibit well-developed canonical-type flat lamellipodia. The localization of ACTN4 to the leading edges was modest (Supplementary Fig. S6). In human invasive lung cancer A549 cells expressing EGFP-ACTN4, ACTN4-enriched lamellipodia similar to those observed in BSC-1 cells were occasionally observed. When A549 cells expressing EGFP-ACTN4 were stimulated with 50 nM phorbol 12-myristate 13-acetate (PMA), ACTN4-enriched ruffle-edge lamellipodia formation was markedly enhanced in a PI3K-dependent manner (Supplementary Fig.S7). To clarify the contribution of ACTN4-enriched ruffle-edge lamellipodia to cell migration, we observed the cell migration process during wound healing of a confluent monolayer culture scraped with a 200 μL pipette tip. Four hours after creating a wound on the coverslip monolayer culture of A549 cells, the cells were fixed with 4%PFA, immunostained for endogenous ACTN4, and observed by fluorescence microscopy and CLEM. Immunofluorescence analysis of ACTN4 showed that ACTN4 was enriched in the leading edge of lamellipodia, extending toward the wounded space. However, in the presence of LY294002, ACTN4-enriched lamellipodia were rarely observed (Supplementary Fig. S8A). Furthermore, CLEM of ACTN4 immunofluorescence and scanning EM clearly demonstrated that ACTN4-enriched lamellipodia have multilayered membrane folds at their leading edges (Supplementary Fig. S8B). Similarly, another highly invasive cancer cell line, human breast cancer MDA-MB-231, also showed ACTN4-enriched lamellipodia formation during wound healing in a PI3K-dependent manner (Supplementary Fig. S9). These findings suggest that ruffle-edge lamellipodia are not present in all cell types, but may be a characteristic feature of certain invasive cancer cells.

***The ruffle-edge lamellipodia formation and cell migration are suppressed by ACTN4 knockdown***

Next, we examined the effect of ACTN4 knockdown on the formation of ruffle-edge lamellipodia and cell migration in A549 cells. Isoform-specific knockdown of ACTNs by ACTN4 or ACTN1

siRNAs was verified by immunofluorescence microscopy and immunoblotting (Supplementary Fig. S10). Five hours after scratching the A549 cell monolayer, cells extending ACTN4-enriched lamellipodia toward the wound space were observed in control siRNA-or ACTN1 siRNA-transfected cells, whereas cells treated with ACTN4 siRNAs did not show marked cell extension (Fig. 7A, Supplementary Fig. S10). CLEM clearly demonstrated that ACTN4 knockdown cells showed only flat protrusions facing the wound space. However, ACTN1 siRNA did not show such an effect on ruffle-edge lamellipodia (Fig. 7B). Furthermore, the wound healing assay demonstrated that cell migration to the scratch wound was significantly reduced by ACTN4 knockdown, but not by ACTN1 knockdown (Fig. 7C). These results indicate a critical role for ACTN4 in cell migration through the formation of ruffle-edge lamellipodia.

***Possible role of the multilayered membrane ruffles at the lamellipodial leading edge in extracellular matrix degradation***

Finally, we investigated the functional significance of the characteristic layered membrane ruffles at the leading edge of lamellipodia. Certain invasive cancer cells invade by forming rod-like protrusions called invadopodia on the ventral surface of the cell, which degrade the ECM, including the basement membrane, by metalloproteases (MPPs). If ruffle-edge lamellipodia are involved in cell invasion, it is possible that MMPs are also localized in the membrane ruffles at the leading edges. Therefore, we examined the localization of MT1-MMP, a major membrane-type MMP, in PMA-stimulated A549 cells by immunofluorescence microscopy. As expected, MT1-MMP was localized to multilayered membranes at the lamellipodial leading edge, where ACTN4 was abundantly localized (Fig. 8A). Additionally, we examined whether A549 cells with ruffle-edge lamellipodia show focal ECM degradation activity on fluorescein isothiocyanate (FITC)-gelatin–coated coverslips. Three hours after plating A549 cells on FITC-gelatin coverslips, the cells produced gelatin degradation areas predominantly located at the leading edge of the lamellipodia (Fig. 8B). Taken together, these observations suggest that ruffle-edge lamellipodia may have ECM degradation activity by MT1-MMP, which localizes in multilayered membranes.

## Discussion

Actinin-1 (ACTN1) and actinin-4 (ACTN4), ubiquitously expressed in non-muscle cells, exhibit high amino acid similarity (87% identity) but show distinct localization and functional roles in cells [21,25,44]. Since its identification by Honda et al. (1998)[25], numerous studies have established that ACTN4 expression is closely associated with cancer invasion and metastasis [31,44–46]. However, the underlying molecular mechanisms are not fully understood.

In this study, we showed that subcellular localization of ACTN4 was most notable in dynamic lamellipodia, whereas ACTN1 was enriched in stress fibers and focal adhesions, and less frequently observed in lamellipodia. Moreover, ACTN4 overexpression significantly increased the proportion of cells with lamellipodia and, in turn, reduced the proportion of cells with stress fibers and focal adhesions. In contrast, overexpression of ACTN1 reduced the proportion of cells with lamellipodia. These results seem to be consistent with those of a previous study showing that ACTN4 overexpression enhances colorectal cancer cell invasion by suppressing focal adhesions and stress fibers [31]. Their study demonstrated that the recruitment of zyxin, a scaffolding protein for focal adhesions, is impaired by ACTN4 overexpression. The reduction in focal adhesions in ACTN4-overexpressing cells can be explained by zyxin-binding-deficient ACTN4 displacement with ACTN1 in focal adhesions.

Furthermore, our live-cell imaging of EGFP-ACTN4 expressing BSC-1 cells and kymograph analysis demonstrated that ACTN4-enriched lamellipodia showed more dynamic advancement than ACTN4-modest lamellipodia. Therefore, ACTN4 may exert its cell migration ability through the formation of ACTN4-enriched lamellipodia. Several studies have suggested a positive correlation between ACTN4 levels and cancer cell motility/invasion [30,47,48]. However, a direct association between ACTN4-enriched lamellipodia and cell migration has not yet been reported. Because phase-contrast microscopy showed that ACTN4-enriched lamellipodia had phase-dark structures at their leading edges, we examined their ultrastructure using CLEM. As expected, CLEM demonstrated that ACTN4-enriched lamellipodia had a unique morphology of multilayered membrane folds at the leading edge. The membrane folds were smaller and more tightly stacked than the membrane ruffles observed in other cell types, including macrophages and EGF-stimulated A431 cells [21,49](Movie 4, Fig. S5). Although conventional membrane ruffles raised by the upward vending of lamellipodia move to the dorsal surface of the cell and sometimes form circular ruffles, which are precursors to macropinosomes, the presence of layered membrane folds is restricted within the narrow area of the lamellipodial edges (Movie 4, 5). More importantly, membrane ruffles in A431 cells and macrophages are resistance to PI3K-inhibitors [20,41], whereas the layered membrane folds of lamellipodial leading edges observed in this study are highly sensitive to PI3K inhibitors. Therefore, the morphology, function, and regulation of layered ruffles at the lamellipodial edges are likely distinct from those of conventional membrane ruffles. We considered ACTN4-enriched lamellipodia

with multilayered ruffles at the leading edge as a new phenotype adapted to active cell migration and termed them "ruffle-edge lamellipodia" as one of the diverse cell membrane protrusions.

Our study demonstrated that ACTN4-enriched ruffle-edge lamellipodia are highly dependent on PI3K activity. PI3K inhibition by LY294002 drastically diminished ACTN4 in lamellipodia and prevented further extension of lamellipodia. Furthermore, high levels of PI(3,4,5)$P_3$, a major product of class I PI3K, were observed in ruffle-edge lamellipodia using fluorescent protein-fused Akt-PH and Btk-PH domains. In contrast, PI3K inhibition did not perturb ACTN4 localization in stress fibers and focal adhesions, where no PI(3,4,5)$P_3$ was detected. Phosphoinositides, particularly PI(4,5)$P_2$ and PI(3,4,5)$P_3$, regulate the activity of several actin-binding proteins [16]. It has been reported that both PI(4,5)$P_2$ and PI(3,4,5)$P_3$ bind to the calponin homology 2 (CH2) domain of ACTN1 but differentially regulate actinin function by modulating the structure and flexibility of the molecule [50,51]. Interestingly, PI(3,4,5)$P_3$ binding to ACTN1 inhibits actin-bunding activity and the interaction between ACTN1 and integrins at focal adhesions [40,52]. As actinin isoforms share highly homologous amino acid sequences, including the CH2 domain, the ACTN4 association with ruffle edge lamellipodia may be mediated by direct binding of PI(3,4,5)$P_3$ to the CH2 domain of ACTN4. PI(3,4,5)$P_3$ -bound ACTN4 may be able to respond to more dynamic movements of the actin network in ruffle-edge lamellipodia. It was also reported that class I PI3K binds to actinin through the p85 subunit [53]. Therefore, ACTN4 can be considered an important downstream effector of class I PI3K in the formation of ruffle-edge lamellipodia, although other PI3K downstream molecules may also be implicated in this process.

It is well-known that Rac1 activation plays a critical role in lamellipodial extension through branched actin network formation by activating the WAVE regulatory complex [17,42,43]. In BSC-1 cells expressing the constitutively active Rac1 Q61L mutant, flat lamellipodia were prominently observed, whereas ACTN4-enriched lamellipodia were rarely observed. In cells expressing a dominant-negative mutant of Rac1 (Rac1T17N), neither flat nor layered-edge lamellipodia were observed. Only BSC-1 cells expressing wild-type Rac1 exhibited ruffle-edge lamellipodia formation. Consistently, the optogenetics of PA-Rac1 also revealed that ACTN4-enriched ruffle-edge lamellipodia changed to ACTN4-modest flat lamellipodia by continuous Rac1 photoactivation. These observations suggest that the local activation-deactivation cycling of Rac1 may be indispensable for ACTN4-enriched ruffle-edge lamellipodia, whereas canonical flat lamellipodia require only Rac1 activation.

Importantly, we confirmed the presence of ruffle-edge lamellipodia in some invasive cancer cells, including A549 lung cancer and MD-MBA-231 human breast cancer cells, but not in all cell types. Because both A549 and MD-MBA-231 cells are known to be representative of highly invasive cancer cells, ACTN4-enriched ruffle-edge lamellipodia may contribute to their invasiveness. ACTN4 knockdown experiments using ACTN4 siRNAs demonstrated that ACTN4 knockdown greatly

suppressed ruffle-edge lamellipodium formation and migration in A549 cells. Thus, it is likely that ACTN4 is essential for progressive cell migration by extending ruffle-edge lamellipodia.

Invasive cancer cells cultured on an artificial extracellular matrix have invadopodia, which are other structures involved in cell invasion. Invadopodia are rod-shaped actin-rich membrane protrusions that arise from the ventral side of the cell and degrade the basal matrix via metalloproteinases (MMPs) [54,55]. Similar to lamellipodia formation, invadopodia are formed through the N-WASP (but not WAVE1 and 2)-Arp2/3 pathway and many actin-binding proteins [56]. Interestingly, it has been reported that overexpression of ACTN4, but not ACTN1, promotes invadopodia formation [57]. In addition, class I PI3K signaling has been shown to be involved in the formation of invadopodia in breast cancer cells [58]. Thus, invadopodia and ACTN-4-enriched ruffle-edge lamellipodia share similarities in the molecular mechanisms of their formation. However, based on their morphology, their functional roles are likely to be distinct. Our live-cell and CLEM imaging demonstrated that ACTN4-enriched lamellipodia have multilayered leading edges and that ACTN4-enriched ruffle-edge lamellipodia aggressively extend in the lateral direction. In contrast, invadopodia extending from ventral cell membranes degrade the basement membrane during cancer cell invasion. Invadopodia and ruffle-edge lamellipodia are likely different cancer invasion modalities with distinct roles: penetration of the basement membrane and invasion of the interstitial tissue by degrading extracellular matrix components, respectively. At the leading edge of lamellipodia, increasing the membrane area through multilayer membrane ruffle formation is advantageous for efficient ECM degradation by MT-MMPs.

**Conclusions**

In conclusion, ACTN4 plays an essential role in ruffle-edge lamellipodia formation in a PI3K-dependent manner. Given its highly characteristic traits, we consider ACTN4-enriched ruffle-edge lamellipodia as a new invasive mode of lamellipodia in certain cell types. Our study emphasizes that ACTN4 may play a critical role in the ability of cells to invade/migrate in the lateral direction through ruffle-edge lamellipodia formation. Further characterization of ACTN4-enriched ruffle-edge lamellipodia would greatly aid in the development of new criteria for cancer cell migration/invasion.

**Acknowledgments**

We are grateful to Drs. Joel A. Swanson (University of Michigan), Klaus Hahn (UNC-Chapel Hill), and Carol Otey (UNC-Chapel Hill) for providing plasmids. We also thank Dr. Eugene Park, Dr. Katsuya Miyake, Mr. Toshitaka Nakagawa, Mr. Kazuhiro Yokoi, and Ms. Yukiko Iwabu for their assistance and advice.

**Funding**

This study was supported by Grants in-Aid from the JSPS (#23K06306 to NA, #20K07245 to YE).

**CRediT authorship contribution statement**

**Haruka Morishita:** Visualization, Validation, Methodology, Investigation, Formal analysis, Data curation, Writing – original draft, Writing - review & editing. **Kawai Katsuhisa:** Methodology, Investigation, Data curation, Writing - review & editing. **Youhei Egami:** Methodology, Investigation, Data curation, Writing - review & editing, Funding acquisition. **Kazufumi Honda:** Resources, Validation, Writing - review & editing. **Nobukazu Araki:** Conceptualization, Project administration, Resources, Visualization, Investigation, Data curation, Writing - original draft; Writing - review & editing; Funding acquisition, Supervision.

**Declaration of Generative AI and AI-assisted technologies in the writing process**

During the preparation of this work, the authors used Paperpal, an AI-assisted academic writing tool, in order to improve readability and language. After using this tool, the authors reviewed and edited the content as needed and take full responsibility for the content of the publication.

**Declaration of Competing Interest**

The authors declare that they have no known competing financial interests or personal relationships that could have appeared to influence the work reported in this paper.

**Data availability**

Most of the data can be found in this article and in the Supporting Information. Additional data are available upon request.

**References**


[1] L.K. Fritz-Laylin, M.A. Titus, The evolution and diversity of actin-dependent cell migration, Mol Biol Cell 34 (2023) pe6. https://doi.org/10.1091/MBC.E22-08-0358/ASSET/IMAGES/LARGE/MBC-34-PE6-G002.JPEG.

[2] M. Ladwein, K. Rottner, On the Rho'd: The regulation of membrane protrusions by Rho-GTPases, FEBS Lett 582 (2008) 2066–2074. https://doi.org/10.1016/J.FEBSLET.2008.04.033.

[3] C. Ballestrem, B. Wehrle-Haller, B. Hinz, B.A. Imhof, Actin-dependent lamellipodia formation and microtubule-dependent tail retraction control-directed cell migration, Mol Biol Cell 11 (2000) 2999–3012. https://doi.org/10.1091/MBC.11.9.2999.

[4] M.L. Gardel, I.C. Schneider, Y. Aratyn-Schaus, C.M. Waterman, Mechanical integration of actin and adhesion dynamics in cell migration, Annu Rev Cell Dev Biol 26 (2010) 315–333. https://doi.org/10.1146/annurev.cellbio.011209.122036.

[5] R.H. Insall, L.M. Machesky, Actin dynamics at the leading edge: from simple machinery to complex networks., Dev Cell 17 (2009) 310–322. https://doi.org/10.1016/j.devcel.2009.08.012.

[6] A.M. Lebensohn, M.W. Kirschner, Activation of the WAVE complex by coincident signals controls actin assembly., Mol Cell 36 (2009) 512–524. https://doi.org/10.1016/j.molcel.2009.10.024.

[7] L.M. Machesky, R.D. Mullins, H.N. Higgs, D.A. Kaiser, L. Blanchoin, R.C. May, M.E. Hall, T.D. Pollard, Scar, a WASp-related protein, activates nucleation of actin filaments by the Arp2/3 complex, Proc Natl Acad Sci U S A 96 (1999) 3739–3744. https://doi.org/10.1073/pnas.96.7.3739.

[8] M. Schaks, G. Giannone, K. Rottner, Actin dynamics in cell migration, Essays Biochem 63 (2019) 483–495. https://doi.org/10.1042/EBC20190015.

[9] C.D. Nobes, A. Hall, Rho, Rac, and Cdc42 GTPases regulate the assembly of multimolecular focal complexes associated with actin stress fibers, lamellipodia, and filopodia, Cell 81 (1995) 53–62. https://doi.org/10.1016/0092-8674(95)90370-4.

[10] A. Mehidi, O. Rossier, M. Schaks, A. Chazeau, F. Binamé, A. Remorino, M. Coppey, Z. Karatas, J.B. Sibarita, K. Rottner, V. Moreau, G. Giannone, Transient Activations of Rac1 at the Lamellipodium Tip Trigger Membrane Protrusion, Current Biology 29 (2019) 2852-2866.e5. https://doi.org/10.1016/J.CUB.2019.07.035.

[11] B. Ding, S. Yang, M. Schaks, Y. Liu, A.J. Brown, K. Rottner, S. Chowdhury, B. Chen, Structures reveal a key mechanism of WAVE regulatory complex activation by Rac1 GTPase, Nature Communications 2022 13:1 13 (2022) 1–13. https://doi.org/10.1038/s41467-022-33174-3.

[12] G. Dimchev, B. Amiri, A.C. Humphries, M. Schaks, V. Dimchev, T.E.B. Stradal, J. Faix, M. Krause, M. Way, M. Falcke, K. Rottner, Lamellipodin tunes cell migration by stabilizing protrusions and promoting adhesion formation, J Cell Sci 133 (2020). https://doi.org/10.1242/JCS.239020.

[13] M. Kaksonen, H.B. Peng, H. Rauvala, Association of cortactin with dynamic actin in lamellipodia and on endosomal vesicles, J Cell Sci 113 Pt 24 (2000) 4421–4426. https://doi.org/10.1242/JCS.113.24.4421.

[14] J.J. Bravo-Cordero, M.A.O. Magalhaes, R.J. Eddy, L. Hodgson, J. Condeelis, Functions of cofilin in cell locomotion and invasion., Nat Rev Mol Cell Biol 14 (2013) 405–415. https://doi.org/10.1038/nrm3609.

[15] G. Giannone, B.J. Dubin-Thaler, O. Rossier, Y. Cai, O. Chaga, G. Jiang, W. Beaver, H.-G. Döbereiner, Y. Freund, G. Borisy, M.P. Sheetz, Lamellipodial actin mechanically links myosin activity with adhesion-site formation., Cell 128 (2007) 561–575. https://doi.org/10.1016/j.cell.2006.12.039.

[16] V. Niggli, Regulation of protein activities by phosphoinositide phosphates, Annu Rev Cell Dev Biol 21 (2005) 57–79. https://doi.org/10.1146/annurev.cellbio.21.021704.102317.

[17] V.S. Kraynov, C. Chamberlain, G.M. Bokoch, M.A. Schwartz, S. Slabaugh, K.M. Hahn, Localized Rac activation dynamics visualized in living cells., Science 290 (2000) 333–7. https://doi.org/10.1126/science.290.5490.333.

[18] T. Kato, K. Kawai, Y. Egami, Y. Kakehi, N. Araki, Rac1-dependent lamellipodial motility in prostate cancer PC-3 cells revealed by optogenetic control of Rac1 activity., PLoS One 9 (2014) e97749. https://doi.org/10.1371/journal.pone.0097749.

[19] T. Oikawa, H. Yamaguchi, T. Itoh, M. Kato, T. Ijuin, D. Yamazaki, S. Suetsugu, T. Takenawa, Ptdlns(3,4,5)P3 binding is necessary for WAVE2-induced formation of lamellipodia, Nat Cell Biol 6 (2004) 420–426. https://doi.org/10.1038/ncb1125.

[20] N. Araki, Y. Egami, Y. Watanabe, T. Hatae, Phosphoinositide metabolism during membrane ruffling and macropinosome formation in EGF-stimulated A431 cells, Exp Cell Res 313 (2007) 1496–1507. https://doi.org/10.1016/J.YEXCR.2007.02.012.

[21] N. Araki, T. Hatae, T. Yamada, S. Hirohashi, Actinin-4 is preferentially involved in circular ruffling and macropinocytosis in mouse macrophages: analysis by fluorescence ratio imaging., J Cell Sci 113 (2000) 3329–3340. http://www.ncbi.nlm.nih.gov/pubmed/10954430.

[22] T. Itoh, J. Hasegawa, Mechanistic insights into the regulation of circular dorsal ruffle formation., J Biochem 153 (2013) 21–9. https://doi.org/10.1093/jb/mvs138.

[23] M. Edlund, M.A. Lotano, C.A. Otey, Dynamics of alpha-actinin in focal adhesions

and stress fibers visualized with alpha-actinin-green fluorescent protein, Cell Motil Cytoskeleton 48 (2001) 190–200. https://doi.org/10.1002/1097-0169(200103)48:3<190::AID-CM1008>3.0.CO;2-C.

[24] B. Kovac, J.L. Teo, T.P. Mäkelä, T. Vallenius, Assembly of non-contractile dorsal stress fibers requires α-actinin-1 and Rac1 in migrating and spreading cells, J Cell Sci 126 (2013) 263–273. https://doi.org/10.1242/jcs.115063.

[25] K. Honda, T. Yamada, R. Endo, Y. Ino, M. Gotoh, H. Tsuda, Y. Yamada, H. Chiba, S. Hirohashi, Actinin-4, a novel actin-bundling protein associated with cell motility and cancer invasion, Journal of Cell Biology 140 (1998) 1383–1393. https://doi.org/10.1083/jcb.140.6.1383.

[26] K.J. Hamill, S.B. Hopkinson, O. Skalli, J.C.R. Jones, Actinin-4 in keratinocytes regulates motility via an effect on lamellipodia stability and matrix adhesions., FASEB J 27 (2013) 546–556. https://doi.org/10.1096/fj.12-217406.

[27] L. Liang, X. Liang, P. Jiang, L. Zhou, L. Zhong, M. Wang, S. Lin, Z. Guo, J. Yu, C. Yang, Y. Chen, C. Zhuo, P. Chen, Y. Wang, Metastasis suppressor 1 interacts with α-actinin 4 to affect its localization and regulate formation of membrane ruffling, Cytoskeleton 78 (2021) 337–348. https://doi.org/10.1002/cm.21686.

[28] D. Tentler, E. Lomert, K. Novitskaya, N.A. Barlev, Role of ACTN4 in Tumorigenesis, Metastasis, and EMT, Cells 8 (2019). https://doi.org/10.3390/cells8111427.

[29] T. Koizumi, H. Nakatsuji, T. Fukawa, S. Avirmed, T. Fukumori, M. Takahashi, H. Kanayama, The Role of Actinin-4 in Bladder Cancer Invasion, Urology 75 (2010). https://doi.org/10.1016/j.urology.2009.09.037.

[30] K. Honda, The biological role of actinin-4 (ACTN4) in malignant phenotypes of cancer, Cell Biosci 5 (2015) 41. https://doi.org/10.1186/s13578-015-0031-0.

[31] M. Fukumoto, S. Kurisu, T. Yamada, T. Takenawa, α-Actinin-4 enhances colorectal cancer cell invasion by suppressing focal adhesion maturation, PLoS One 10 (2015) e0120616. https://doi.org/10.1371/journal.pone.0120616.

[32] S. Yamada, S. Yanamoto, H. Yoshida, I. Yoshitomi, G. Kawasaki, A. Mizuno, T.K. Nemoto, RNAi-mediated down-regulation of α-actinin-4 decreases invasion potential in oral squamous cell carcinoma, Int J Oral Maxillofac Surg 39 (2010). https://doi.org/10.1016/j.ijom.2009.10.003.

[33] K. Honda, Development of Biomarkers to Predict Recurrence by Determining the Metastatic Ability of Cancer Cells, J Nippon Med Sch 89 (2022) 24–32. https://doi.org/10.1272/JNMS.JNMS.2022_89-118.

[34] N. Araki, Y. Ikeda, T. Kato, K. Kawai, Y. Egami, K. Miyake, N. Tsurumaki, M. Yamaguchi, Development of an automated fluorescence microscopy system for

photomanipulation of genetically encoded photoactivatable proteins (optogenetics) in live cells, Microscopy 63 (2014) 255–260. https://doi.org/10.1093/jmicro/dfu003.

[35] M. Fujii, K. Kawai, Y. Egami, N. Araki, Dissecting the roles of Rac1 activation and deactivation in macropinocytosis using microscopic photo-manipulation, Sci Rep 3 (2013) 2385. https://doi.org/10.1038/srep02385.

[36] Y.I. Wu, D. Frey, O.I. Lungu, A. Jaehrig, I. Schlichting, B. Kuhlman, K.M. Hahn, A genetically encoded photoactivatable Rac controls the motility of living cells., Nature 461 (2009) 104–8. https://doi.org/10.1038/nature08241.

[37] Y. Ikeda, K. Kawai, A. Ikawa, K. Kawamoto, Y. Egami, N. Araki, Rac1 switching at the right time and location is essential for Fc$\gamma$ receptor-mediated phagosome formation, J Cell Sci 130 (2017) 2530–2540. https://doi.org/10.1242/jcs.201749.

[38] A. Simonsen, A.E. Wurmser, S.D. Emr, H. Stenmark, The role of phosphoinositides in membrane transport, Curr Opin Cell Biol 13 (2001) 485–492. https://doi.org/10.1016/S0955-0674(00)00240-4.

[39] M.A. De Matteis, A. Godi, PI-loting membrane traffic, Nat Cell Biol 6 (2004) 487–492. https://doi.org/10.1038/ncb0604-487.

[40] T.S. Fraley, T.C. Tran, A.M. Corgan, C.A. Nash, J. Hao, D.R. Critchley, J.A. Greenwood, Phosphoinositide binding inhibits $\alpha$-actinin bundling activity, J Biol Chem 278 (2003) 24039–24045. https://doi.org/10.1074/jbc.M213288200.

[41] N. Araki, M.T. Johnson, J.A. Swanson, A role for phosphoinositide 3-kinase in the completion of macropinocytosis and phagocytosis by macrophages., J Cell Biol 135 (1996) 1249–60. https://doi.org/10.1083/jcb.135.5.1249.

[42] A.J. Ridley, Historical overview of Rho GTPases., Methods Mol Biol 827 (2012) 3–12. https://doi.org/10.1007/978-1-61779-442-1_1.

[43] A.J. Ridley, Rho GTPases and cell migration., J Cell Sci 114 (2001) 2713–2722.

[44] K.S. Hsu, H.Y. Kao, Alpha-Actinin 4 and Tumorigenesis of Breast Cancer, in: Vitam Horm, Academic Press Inc., 2013: pp. 323–351. https://doi.org/10.1016/B978-0-12-416673-8.00005-8.

[45] X. Liu, K.M. Chu, $\alpha$-Actinin-4 promotes metastasis in gastric cancer, Lab Invest 97 (2017) 1084–1094. https://doi.org/10.1038/LABINVEST.2017.28.

[46] H. Yoshii, K. Ito, T. Asano, A. Horiguchi, M. Hayakawa, T. Asano, Increased expression of $\alpha$-actinin-4 is associated with unfavorable pathological features and invasiveness of bladder cancer, Oncol Rep 30 (2013) 1073–1080. https://doi.org/10.3892/OR.2013.2577.

[47] A. Barai, A. Mukherjee, A. Das, N. Saxena, S. Sen, $\alpha$-Actinin-4 drives invasiveness by regulating myosin IIB expression and myosin IIA localization, J Cell Sci 134

(2021). https://doi.org/10.1242/JCS.258581.

[48] M.C. Wang, Y.H. Chang, C.C. Wu, Y.C. Tyan, H.C. Chang, Y.G. Goan, W.W. Lai, P.N. Cheng, P.C. Liao, Alpha-actinin 4 is associated with cancer cell motility and is a potential biomarker in non-small cell lung cancer, Journal of Thoracic Oncology 10 (2015) 286–301. https://doi.org/10.1097/JTO.0000000000000396.

[49] M. Maekawa, S. Terasaka, Y. Mochizuki, K. Kawai, Y. Ikeda, N. Araki, E.Y. Skolnik, T. Taguchi, H. Arai, Sequential breakdown of 3-phosphorylated phosphoinositides is essential for the completion of macropinocytosis., Proc Natl Acad Sci U S A 111 (2014) E978-87. https://doi.org/10.1073/pnas.1311029111.

[50] A.M. Corgan, C. Singleton, C.B. Santoso, J.A. Greenwood, Phosphoinositides differentially regulate α-actinin flexibility and function, Biochem J 378 (2004) 1067–1072. https://doi.org/10.1042/BJ20031124.

[51] S.J. Full, M.L. Deinzer, P.S. Ho, J.A. Greenwood, Phosphoinositide binding regulates α-actinin CH2 domain structure: Analysis by hydrogen/deuterium exchange mass spectrometry, Protein Science 16 (2007) 2597–2604. https://doi.org/10.1110/ps.073146807.

[52] J.A. Greenwood, A.B. Theibert, G.D. Prestwich, J.E. Murphy-Ullrich, Restructuring of Focal Adhesion Plaques by Pi 3-Kinase, J Cell Biol 150 (2000) 627–642. https://doi.org/10.1083/jcb.150.3.627.

[53] F. Shibasaki, K. Fukami, Y. Fukui, T. Takenawa, Phosphatidylinositol 3-kinase binds to alpha-actinin through the p85 subunit., Biochem J 302 ( Pt 2) (1994) 551–557. https://doi.org/10.1042/BJ3020551.

[54] D.A. Murphy, S.A. Courtneidge, The “ins” and “outs” of podosomes and invadopodia: characteristics, formation and function, Nat Rev Mol Cell Biol 12 (2011) 413–426. https://doi.org/10.1038/nrm3141.

[55] R. Buccione, J.D. Orth, M.A. McNiven, Foot and mouth: podosomes, invadopodia and circular dorsal ruffles, Nat Rev Mol Cell Biol 5 (2004) 647–657. https://doi.org/10.1038/NRM1436.

[56] H. Yamaguchi, M. Lorenz, S. Kempiak, C. Sarmiento, S. Coniglio, M. Symons, J. Segall, R. Eddy, H. Miki, T. Takenawa, J. Condeelis, Molecular mechanisms of invadopodium formation: The role of the N-WASP-Arp2/3 complex pathway and cofilin, J Cell Biol 168 (2005) 441–452. https://doi.org/10.1083/jcb.200407076.

[57] H. Yamaguchi, Y. Ito, N. Miura, Y. Nagamura, A. Nakabo, K. Fukami, K. Honda, R. Sakai, Actinin-1 and actinin-4 play essential but distinct roles in invadopodia formation by carcinoma cells, Eur J Cell Biol 96 (2017) 685–694. https://doi.org/10.1016/j.ejcb.2017.07.005.

[58] H. Yamaguchi, S. Yoshida, E. Muroi, N. Yoshida, M. Kawamura, Z. Kouchi, Y. Nakamura, R. Sakai, K. Fukami, Phosphoinositide 3-kinase signaling pathway mediated by p110 $\alpha$ regulates invadopodia formation, J Cell Biol 193 (2011) 1275–1288. https://doi.org/10.1083/jcb.201009126.

**Legends of Figures**

**Figure 1. Confocal microscopy showing endogenous ACTN4 localization and F-actin distribution in control BSC-1 cells (A) and LY294002-treated cells (B).** Cells were fixed and immunostained with an anti-ACTN4 antibody, followed by an Alexa Fluor 488-labeled secondary antibody. F-actin was detected using Alexa Fluor 568-phalloidin. (A) In control cells, ACTN4 was localized to lamellipodia, actin stress fibers, and focal adhesions. Three boxed areas (a, b, and c in the ACTN4 image) are magnified in the lower column. (B) In cells pretreated with 25 μM LY294002 for 20 min, ACTN4-enriched lamellipodia were scarcely observed, although ACTN4 localization in stress fibers and focal adhesions was evident. Magnified images of the boxed areas are shown below. DIC, differential interference contrast images. Scale bars, 10 μm. (C) The percentage of cells showing three ACTN4 localization types, L-type, I-type SF-type, was calculated by counting >60 cells on each coverslip for the control and LY294002 (LY)-treated cells. n=6 coverslips from three independent experiments. $^{**}P<0.01$.

**Figure 2. Overexpression of ACTN4, but not ACTN1, enhances ACTN-enriched lamellipodial formation in a PI3K-dependent manner.** According to the ACTN localization pattern, BSC-1 cells transfected with pEGFP-ACTN4 were classified into three types: lamellipodia localization predominant (L)-type (A), intermediate (I)-type (B), and stress fiber localization predominant (SF)-type (C). In contrast, the SF-type cells were most abundant in EGFP-ACTN1 overexpressing cells (D). (E) Percentages of cells showing three ACTN localization types, L-type (red bars), I-type (orange), and SF-type (blue), in ACTN4- or ACTN1-overexpressing cells before and after the addition of LY294002 (LY). $^{**}P<0.01$, n＝６. (F) EGFP-ACTN4 was markedly diminished in the lamellipodium after the addition of LY294002. Linescan analysis (right panel) along the dotted line in the left images shows a decrease in the fluorescence intensity of EGFP-ACTN4 in lamellipodia after the addition of LY294002. The corresponding movie is available in the supplementary materials (Movie 3). All scale bars, 10 μm.

**Figure 3. EGFP-ACTN4 was diminished almost simultaneously with mCherry-Akt-PH domain (Akt-PH) monitoring PI(3,4,5)$P_3$ and PI(3,4)$P_2$ by the addition of 25 μM LY294002 (LY).** (A) Time-lapse images of live-BSC-1 cells co-expressing EGFP-ACTN4 and mCherry-Akt-PH. Eight minutes after the start of time-lapse imaging, LY was added to the cells. Arrowheads indicate that ACTN4 localizes in focal adhesions and stress fibers even after LY addition. The times elapsed from the first frame acquisition are shown in the upper-left corner. (B) Kymographs from the time series along the white line in Akt-PH and ACTN4 images of A. The constructed kymographs depict the trajectory of lamellipodial movement and fluorescent signals. Rows of pixels at the line are laid side-by-side in a montage to create a time (*T*) vs. distance (*D*) plot. Both fluorescent signals of Akt-PH and ACTN4 diminished almost simultaneously within a few minutes of LY addition. The arrow indicates the time point of LY addition. Scale bar, 10 μm.

**Figure 4. Comparison of the dynamics of ACTN4-enriched and ACTN4-modest lamellipodia in BSC-1 cells.** The left cell shows ACTN4-modest lamellipodia (a). The right cell has an ACTN4-enriched lamellipodium, in which the leading edge shows a wavy appearance (b). Scale bar: 10 μm. **(B)** Kymograph analysis of ACTN4-modest (arrow, a) and ACTN4-enriched lamellipodia (arrow, b). Comparing ACTN4-modest lamellipodia and ACTN4-enriched lamellipodia, the moving speed of ACTN4-enriched lamellipodia was significantly faster than that of ACTN4-modest lamellipodia **(B, C)**. ACTN4-enriched lamellipodia always extended forward at an average speed of 0.37±0.15 μm /min (n= 15 lamellipodia collected from 3-independent experiments), whereas ACTN4-modest flat lamellipodia moved with repeated extension and retraction at an average speed of 0.07±0.04 μm /min (n=15 lamellipodia collected from 3-independent experiments). $^{**}P<0.01$.

**Figure 5. Correlative light-electron microscopy (CLEM) of EGFP-ACTN4-enriched lamellipodia.** (A) Fluorescence microscopic image of EGFP-ACTN4 in a BSC-1 cell. (B) The ACTN4 image was overlaid on the scanning EM image of the same cell to identify ACTN4-enriched lamellipodia. Scanning electron micrographs of the boxed regions in B are magnified in the lower panels (C, D). Note that ACTN4-enriched lamellipodia have multilayered membranes at the leading edge. Scale bars, 10 μm.

**Figure 6. Rac1 cycling is indispensable for ACTN4-enriched lamellipodia.** (A) BSC-1 cells were transfected with pmCitrine-Rac1 of wild type (WT), constitutively active mutant (Q61L), or dominant negative mutant (T17N). After fixation, ACTN4 was detected by immunostaining with an anti-ACTN4 antibody, followed by an Alexa Fluor 594-labeled secondary antibody. ACTN4-enriched lamellipodia are remarkable in cells expressing Rac1 WT. In cells expressing constitutively active Rac1 Q61L, flat leading-edge lamellipodia were prominent around the cell perimeter. Rac1 T17N expressing cells scarcely have lamellipodia (open arrow), although the next non-expressing cells have ACTN4-enriched lamellipodia (arrow). (B) Representative time-lapse images showing that continuous photoactivation of PA-Rac1 changed the lamellipodia phenotype from ACTN4-enriched layered-edge lamellipodia to flat-edge lamellipodia (arrows). Insets show line scan analysis of EGFP-ACTN4 fluorescence intensity at the red dotted line in the lamellipodia. Continuous activation of PA-Rac1 decreased EGFP-ACTN4 fluorescence intensity in lamellipodia. Scale bars, 10 μm.

**Figure 7. ACTN4 knockdown suppressed the layered-edge lamellipodium formation and cell migration in A549 cells.** (A) A549 cells subconfluently cultured on coverslips were transfected with negative control (NC) siRNA, ACTN4 siRNA (#1-3), or ACTN1 siRNA. After 48 h of transfection, the monolayer culture was scratched with a 200 μL pipette tip to make a wound and incubated for 5 h in the presence of 50 nM PMA. After fixation, ACTN4 was detected by immunofluorescence. F-actin and nuclei were stained with Alexa Fluor 568-phalloidin and DAPI, respectively. Fluorescence microscopy demonstrated that ACTN4-enriched lamellipodia extended to the scratched wound space

of the monolayer culture in which cells were treated with NC siRNA or ACTN1 siRNA (arrowheads). However, lamellipodial extension was hardly observed in ACTN4 knockdown cells by ACTN4 siRNA#1. Asterisks denote the wounded space. Scale bars, 10 μm. (B) CLEM of ACTN4 fluorescence and scanning electron microscopy (SEM) reveals that isoform-specific knockdown of ACTN4 by siRNA inhibits layered-edge lamellipodia formation during cell migration. After fluorescence microscopy, cells were processed to scanning EM. The same area as ACTN4 fluorescence micrograph was photographed by SEM, and the two images were superimposed using Adobe Photoshop. Arrowheads indicate ACTN4-enriched layered-edge lamellipodia in A549 cells transfected with NC or ACTN1 siRNA. In ACTN4 KD cells by ACTN4 siRNAs, only flat thin lamellipodia were seen (open arrows). Similar results were obtained in cells transfected with ACTN4 siRNAs #2 and #3. Scale bars: 10 μm. (C) Wound healing assay demonstrating that ACTN4 knockdown perturbed the migration capacity of A549 cells. Representative images of scratched and recovering wounded areas at indicated times (black lines) on confluent monolayers of cancer cells treated with NC siRNA or ACTN4 siRNA (left image). Cell migration capacity was determined by measuring the migration distance by subtracting the width of the wounds at 5 h (blue lines) after making the wounds on cell monolayers from that at 0 h (yellow broken lines). Graph data are presented as fold-changes relative to the migration distance of NC siRNA-treated cells. ACTN4-KD cells showed a significantly lower migration capacity than ACTN1-KD or control cells (*$P<0.05$, n=3). Values are expressed as means ± SEM of three independent experiments.

**Figure 8. MT1-MMP localization and gelatin degradation activity of ruffle-edge lamellipodia.** (A) PMA-stimulated A549 cells were immunolabeled for endogenous MT1-MMP (red) and ACTN4 (green). MT1-MMP localizes to ACTN4-enriched ruffle-edge lamellipodia (arrows). DAPI, nuclear stain. (B) A549 cells were plated onto FITC-gelatin-coated coverslips and incubated for 3 h in the presence of 100 nM PMA. After fixation with 4%PFA, F-actin was stained with Alexa Fluor 568-phalloidin. FITC-gelatin degradation activity was observed as dark areas beneath lamellipodia tips. Scale bars, 10 μm.

**Appendix A. Supplementary information**

**Supplementary Figure S1. High-resolution confocal microscopy showing the representative localization of ACTN4 in L-type BSC-1 cells.** BSC-1 cells transfected with EGFP-ACTN4 were fixed with 4% PFA. F-actin was stained with Alexa Fluor 568 phalloidin. Nuclei were stained with DAPI. High-resolution images were acquired with the Nikon AX NSPARC confocal laser microscope system. ACTN4 was observed to be associated with wavy membranous structures at the leading edge of lamellipodium. Actin stress fibers were not observed in L-type cells. The blue-boxed region was enlarged in the lower frame. Scale bars: 10 μm.

**Supplementary Figure S2. High-resolution confocal microscopy showing the representative localization of ACTN1 in control BSC-1 cells (A) and LY294002-treated cells (B).** BSC-1 cells transfected with EGFP-ACTN1 were treated with LY294002, followed by fixation with 4% PFA. Cells were immunostained with an anti-vinculin antibody, which labels focal adhesions. F-actin was stained with Acti-stain 670. Images were acquired with the Nikon AX NSPARC confocal laser microscope system. (A) ACTN1 was localized to actin stress fibers and focal adhesions (arrows) in control BSC-1 cells. Localization of ACTN1 to lamellipodia (open arrow) was modest. (B) The localizations of ACTN1 in actin stress fibers and focal adhesions (arrows) was not diminished by the LY294002 treatment. Scale bars: 10 μm.

**Supplementary Figure S3. High-resolution confocal microscopy showing the representative localization of ACTN4 in LY294002-treated BSC-1 cells.** BSC-1 cells transfected with EGFP-ACTN4 were treated with 25 μM LY294002 for 30 min and fixed with 4%PFA. Cells were immunostained with an anti-vinculin antibody, which labels focal adhesions. F-actin was stained with Acti-stain 670. Images were acquired with the Nikon AX NSPARC confocal laser microscope system. After LY294002 treatment, the localization of ACTN4 in lamellipodia was markedly diminished, while ACTN4 in actin stress fibers and focal adhesions (arrows) was sustained. Scale bars: 10 μm.

**Supplementary Figure S4. Effect of LY294002 on 3' phosphoinositide in lamellipodial leading edges.** (A) BSC-1 cells were co-transfected with mCitrine-Akt-PH and mCherry-membrane (Mem). Ratio images of Akt-PH/Mem showing that PI(3,4,5)$P_3$/PI83,4$P_2$ concentrations in the plasma membrane were created by the MetaMorph imaging system, as previously described [21]. Note that PI(3,4,5)$P_3$/PI83,4$P_2$ concentrations in the membrane of lamellipodial leading edges (arrows) decreased by the addition of 25 μM LY294002 (LY). (B) Live-cell microscopy of a BSC1 cell showing the effect of LY294002 on lamellipodia enriched with PI(3,4,5)$P_3$ monitored with YFP-Btk PH domain. In BSC-1 cells expressing YFP-Btk PH domain, PI(3,4,5)$P_3$ was detected at the leading

edge of lamellipodium (arrows). After the addition of LY, PI(3,4,5)$P_3$ markedly diminished in the lamellipodium. The corresponding phase-contrast images are shown in the left frame. It is also notable that the phase-dark structures at the leading edge of the lamellipodium disappeared after the addition of LY (open arrows). Scale bars: 10 μm. A corresponding movie is available in the supplementary materials (Movie 2).

**Supplementary Figure S5. Scanning EM showing that ruffle-edge lamellipodia are distinct from membrane ruffles arising from flat lamellipodia in RAW264 macrophages and EGF-stimulated A431 cells.** Multi-layered membrane ruffles of lamellipodial leading edge in BSC-1 cells are smaller and more tightly stacked than membrane ruffles in RAW264 and EGF-stimulated A431 cells. Membrane ruffles arising from flat lamellipodia extend to the dorsal surface of RAW264 and A431 cells (arrows), whereas the presence of layered membrane ruffles is restricted to within ~3 μm of the leading edge of the lamellipodium (upper right enlarged image of the boxed area) in BSC-1 cells. Scale bars: 10 μm.

**Supplementary Figure S6. ACTN4-enriched layered-edge lamellipodia were rarely observed in HeLa, MDCK II, or B16 cells.** Live cells transfected with EGFP-ACTN4 were observed by phase-contrast and fluorescence microscopy. In HeLa cells, ACTN4 was predominantly localized in stress fibers and focal adhesions. Although MDCK II cells frequently showed the extension of lamellipodia (arrows), they did not have ACTN4-enriched ruffle edge. B16 cells showed well-developed lamellipodia (open arrow), but the ACTN4 localization in their flat leading edges was modest. Scale bars: 10 μm.

**Supplementary Figure S7. Presence of ACTN4-enriched ruffle-edge lamellipodia in A549 cells stimulated with PMA.** (A) By live-cell imaging of A549 cells transfected with EGFP-ACTN4, ACTN4-enriched lamellipodia were frequently observed in PMA-stimulated A549 cells (upper column). ACTN4-enriched lamellipodia diminished with the addition of LY294002 (lower column). Scale bar: 10 μm. (B) Scanning EM showing that lamellipodia have multilayered membrane folds at their leading edges in PMA-stimulated A549 cells. A magnified view of the boxed area is shown in the right frame. Scale bars: 5 μm.

**Supplementary Fig. S8. Formation of ACTN4-enriched layered ruffle-edge lamellipodia during wound healing in human non-small cell lung cancer A549 cell monolayer culture.** (A) Three hours after creating a wound on the monolayer culture, the cells were fixed with PFA. Endogenous ACTN4 was immunostained with an anti-ACTN4 antibody, followed by Alexa Fluor 488-labeled secondary antibody (green). F-actin was stained with Alexa Fluor 568-phalloidin (red). Nuclei were stained with DAPI (blue). In phorbol 12-myristate 13-acetate (PMA)-stimulated A549 cells,

ACTN4-enriched lamellipodia (arrows) were formed in migrating cells toward the wounded space (asterisks). The formation of ACTN4-enriched lamellipodia was inhibited by LY294002 (LY) treatment (open arrows). (B) CLEM reveals that ACTN4-enriched lamellipodia protruding toward the wounded space (asterisks) have multilayered membrane folds at their leading edges. A magnified view of the boxed area is shown in the right frame. Scale bars: 10 μm.

**Supplementary Figure S9. Formation of ACTN4-enriched layered ruffle-edge lamellipodia during wound healing of human invasive breast cancer MDA-MB-231 cell monolayer culture.** (A) Three hours after creating a wound on the monolayer culture, cells were fixed and stained with anti-ACTN4 (green) and Alexa Fluor 564-phalloidine (red). In control MDA-MB-231 cells, ACTN4-enriced lamellipodia were formed in migrating cells toward the wounded space (arrows). ACTN4-enriched lamellipodia were not observed after LY294002 treatment (open arrows). Scale bars: 10 μm. (B) Scanning EM reveals that lamellipodia extending toward the wounded space have multilayered membrane folds (arrow). Scale bars: 10 μm.

**Supplementary Figure S10. Isoform-specific knockdown of ACTN4 by siRNA.** (A) A549 cells subconfluently cultured on coverslips were transfected with negative control (NC) siRNA, three ACTN4 siRNAs (#1, #2, #3), or ACTN1 siRNA. Five hours after scratching the monolayer of culture cells, the cells were fixed and subjected to ACTN4 immunocytochemistry and F-actin staining. Nuclei were stained with DAPI. Scale bars: 20 μm. (B) Expression levels of ACTN4 were quantified using immunofluorescence intensities measured by the MetaMorph imaging software. The average fluorescence intensity values in >8 cell areas facing the wounded space in each coverslip were calculated. ACTN4 fluorescence intensity was normalized to the intensity of NC siRNA-transfected cells after background correction. ACTN4 siRNA (#1-3), but not ACTN1 siRNA, significantly reduced ACTN4 protein expression (**$P$<0.01, n=3). Values are expressed as the means ± SEM of triplicate experiments and are representative of two other independent experiments. The fluorescent intensity in representative images was shown in the cell area (dotted line in A). (C) Immunoblot analysis with anti-ACTN4 or anti-ACTN1 antibodies demonstrated that ACTN4 siRNAs #1-3 reduce ACTN4 protein levels, but not ACTN1 protein levels. Immunoblotting with an anti-GAPDH antibody verified equal amounts of total protein loading.

**Movie 1. Live-cell movie showing the effect of LY294002 on EGFP-ACTN4 localization in BSC-1 cells.** Phase-contrast and fluorescence images of BSC-1 cells expressing EGFP-ACTN4 and mCherry-Lifeact were acquired at 15 s intervals for 20 min. EGFP-ACTN4 in the leading edges of lamellipodia markedly decreased within 5 min of the addition of LY294002 (white arrows), whereas that in the stress fibers and focal adhesions was sustained (blue arrows). The elapsed time after the

addition of LY294002 is shown in the upper-left corner of the frame. 90× speed. Scale bars: 10 μm.

**Movie 2. Live-cell movie showing the effect of LY294002 on lamellipodia enriched with PI(3,4,5)$P_3$ monitored with YFP-Btk PH domain (right frame).** PI(3,4,5)$P_3$ is found to be enriched at the leading edge of the lamellipodia. LY294009 was added at the time point 8 min. The addition of LY294002 decreased PI(3,4,5)$P_3$ levels in lamellipodia. The corresponding phase-contrast image is shown on the left-hand side of the figure. 90× speed. Scale bars: 10 μm.

**Movie 3. Live-cell movie of EGFP-ACTN4 (right) and the corresponding DIC (left) images in BSC-1 cells.** The cell on the right side has an ACTN4-enriched lamellipodium, in which the leading edge shows a wavy appearance (arrow in the DIC images). The ACTN4-enriched lamellipodium (arrow) progressively extends, whereas the ACTN4-modest flat lamellipodia-like protrusions (open arrows) in the cell on the left side are not motile. 90× speed. Scale bars: 10 μm.

**Movie 4. Phase-dark wavy structures at the lamellipodial leading edge in BSC-1 cells are distinct from membrane ruffling in m-CSF-stimulated RAW264 cells and EGF-stimulated A431 cells.** Membrane ruffles observed in RAW and A431 cells are mostly single lamellar structures originating from the cell periphery and move to the dorsal surface (black arrows). Wavy structures in BSC-1 cells are smaller and restricted to the narrow region of the lamellipodial leading edges (red arrows). 180× speed. Scale bars: 10 μm.

**Movie 5. Long-term movie of an EGFP-ACTN4-expressing BSC-1 cell showing active cell migration through extending lamellipodia with phase-dark wavy edges.** After confirming EGFP-ACTN4 expression, phase-contrast images of the cell were acquired at 30 s intervals for 17 h. This ACTN4-expressing cell frequently forms lamellipodia, but their presence is temporary. The playback speed is displayed in the movie frame. Scale bars: 10 μm.

**Movie 6. Optogenetic activation of PA-Rac1 induces a morphological change from ACTN4-enriched layered-edge lamellipodia to ACTN4-modest flat lamellipodia exhibiting larger ruffling movement.** BSC-1 cells co-transfected with EGFP-ACTN4 and mCherry-LOV2-Rac1Q61L were subjected to PA-Rac1 photoactivation by blue light irradiation. Before photoactivation, the cells have ACTN4-enriched layered-edge lamellipodia (arrows), which is a phenotype of endogenous wild-type Rac1. Photoactivation of PA-Rac1 transformed ruffle-edge lamellipodia to flat lamellipodia within several minutes. The elapsed time after PA-Rac1 photoactivation is shown in the frame. 90× speed. Scale bars: 10 μm.

# Figure 1

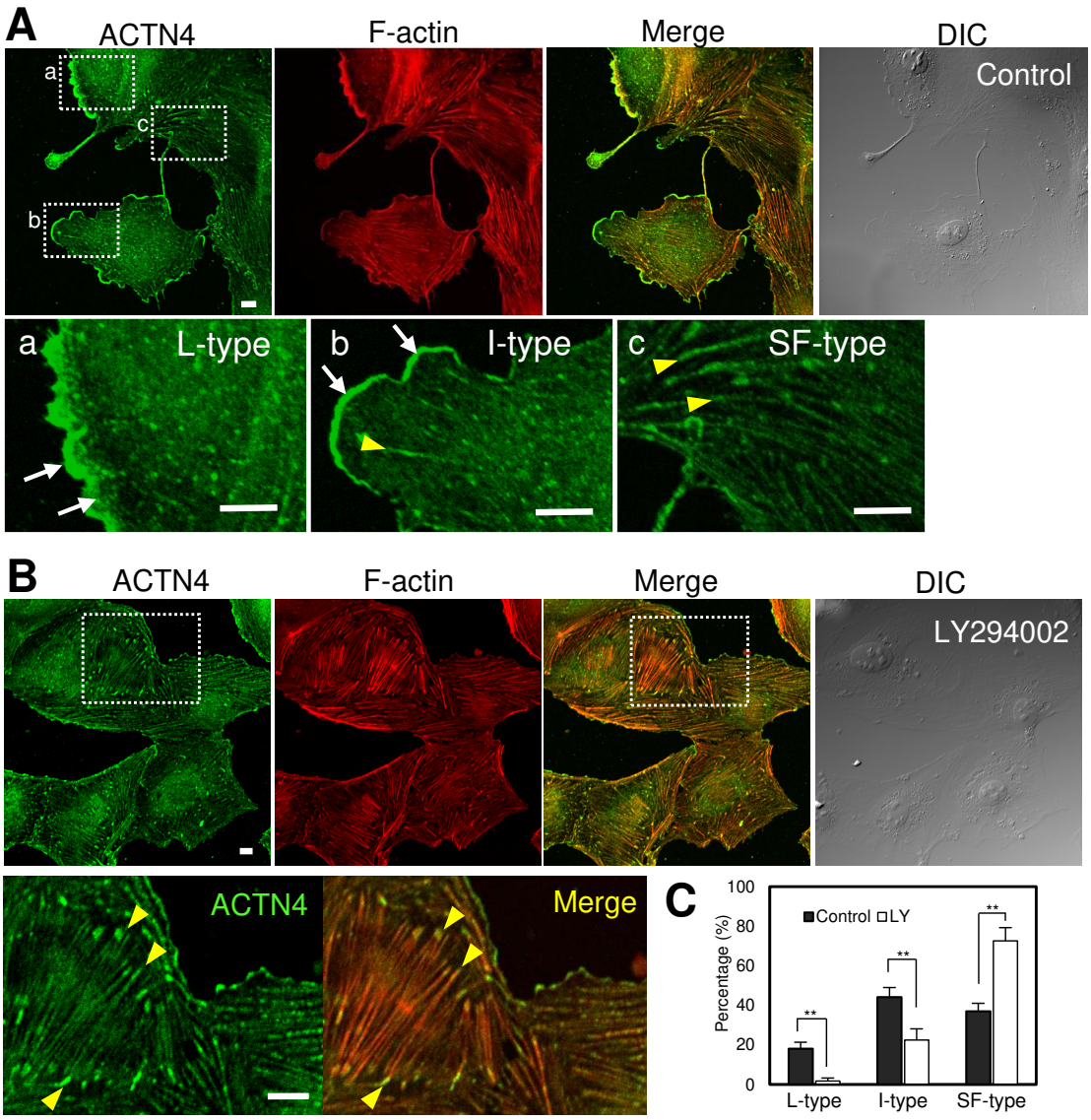
A
ACTN4
F-actin
Merge
DIC
Control
a
b
c
L-type
I-type
SF-type
B
ACTN4
F-actin
Merge
DIC
LY294002
ACTN4
Merge
C
Control
LY
Percentage (%)
100
80
60
40
20
0
**
L-type
I-type
SF-type

# Figure 2

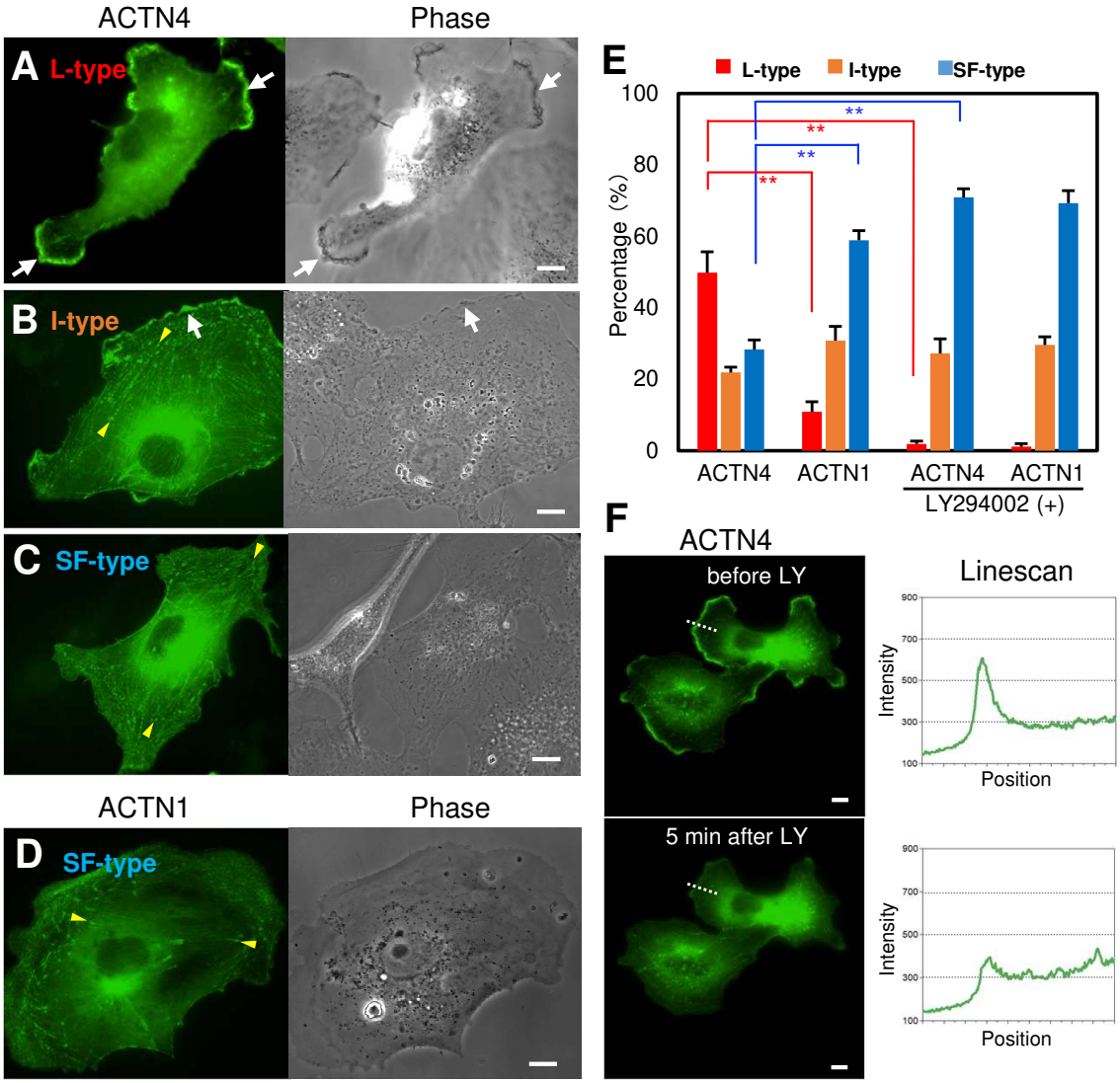
ACTN4
Phase
A L-type
B I-type
C SF-type
ACTN1
Phase
D SF-type
E
L-type
I-type
SF-type
Percentage (%)
100
80
60
40
20
0
**
ACTN4
ACTN1
ACTN4
ACTN1
LY294002 (+)
F
ACTN4
before LY
5 min after LY
Linescan
Intensity
Position

# Figure 3

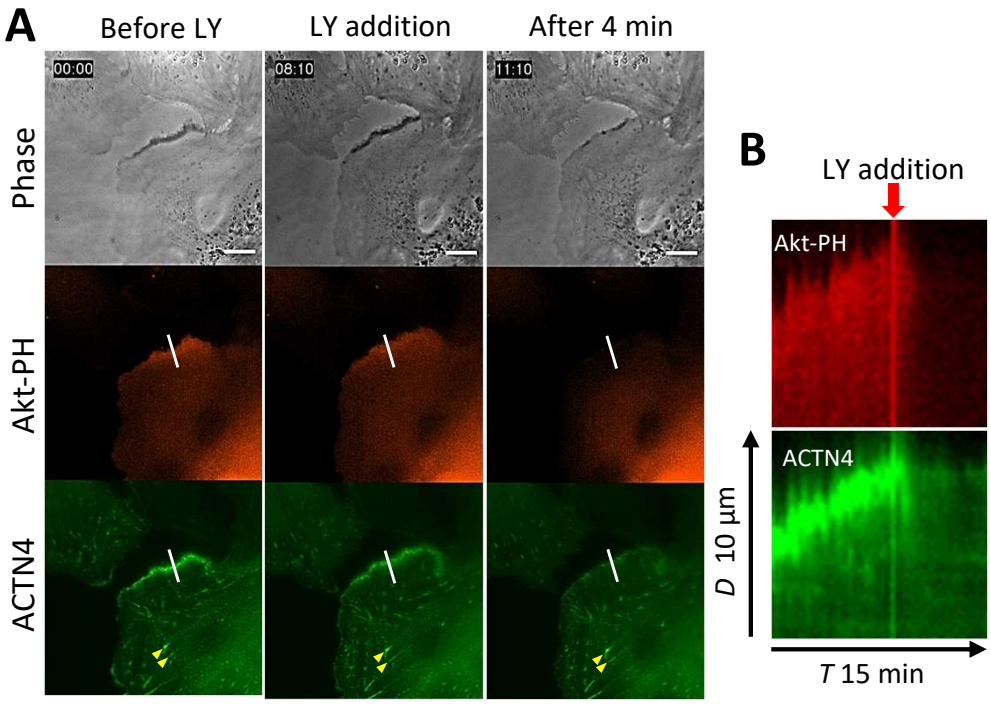
A
Before LY
LY addition
After 4 min
00:00
08:10
11:10
Phase
Akt-PH
ACTN4
B
LY addition
Akt-PH
ACTN4
D 10 µm
T 15 min

# Figure 4

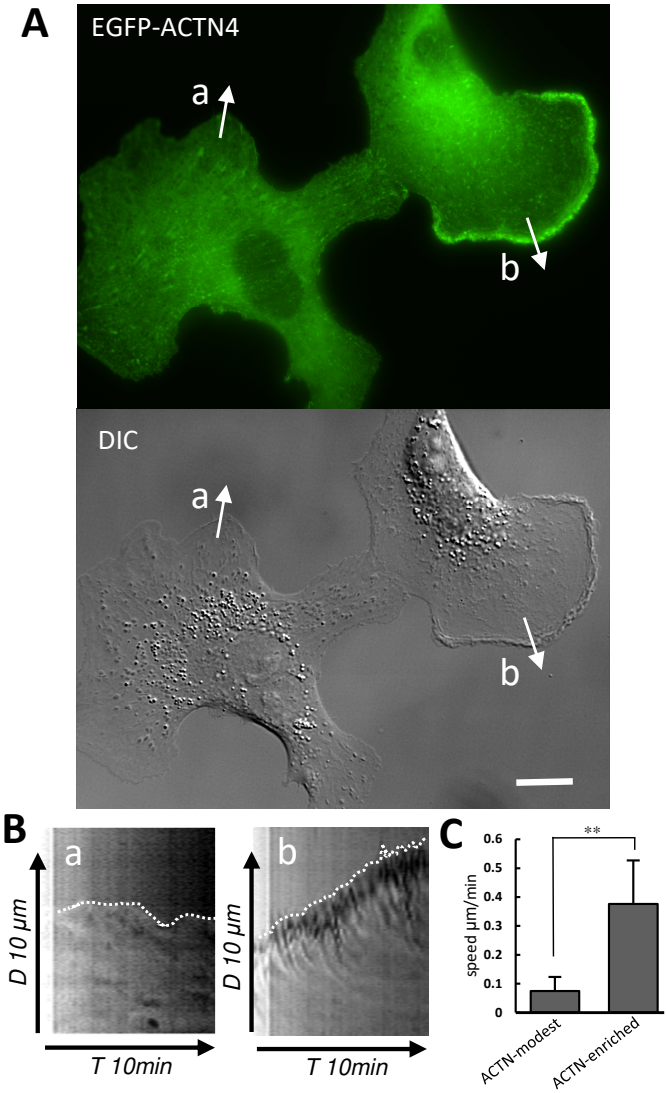
A
EGFP-ACTN4
a
b
DIC
a
b
B
a
D 10 µm
T 10min
b
D 10 µm
T 10min
C
**
speed µm/min
0.6
0.5
0.4
0.3
0.2
0.1
0
ACTN-modest
ACTN-enriched

**Figure 5**

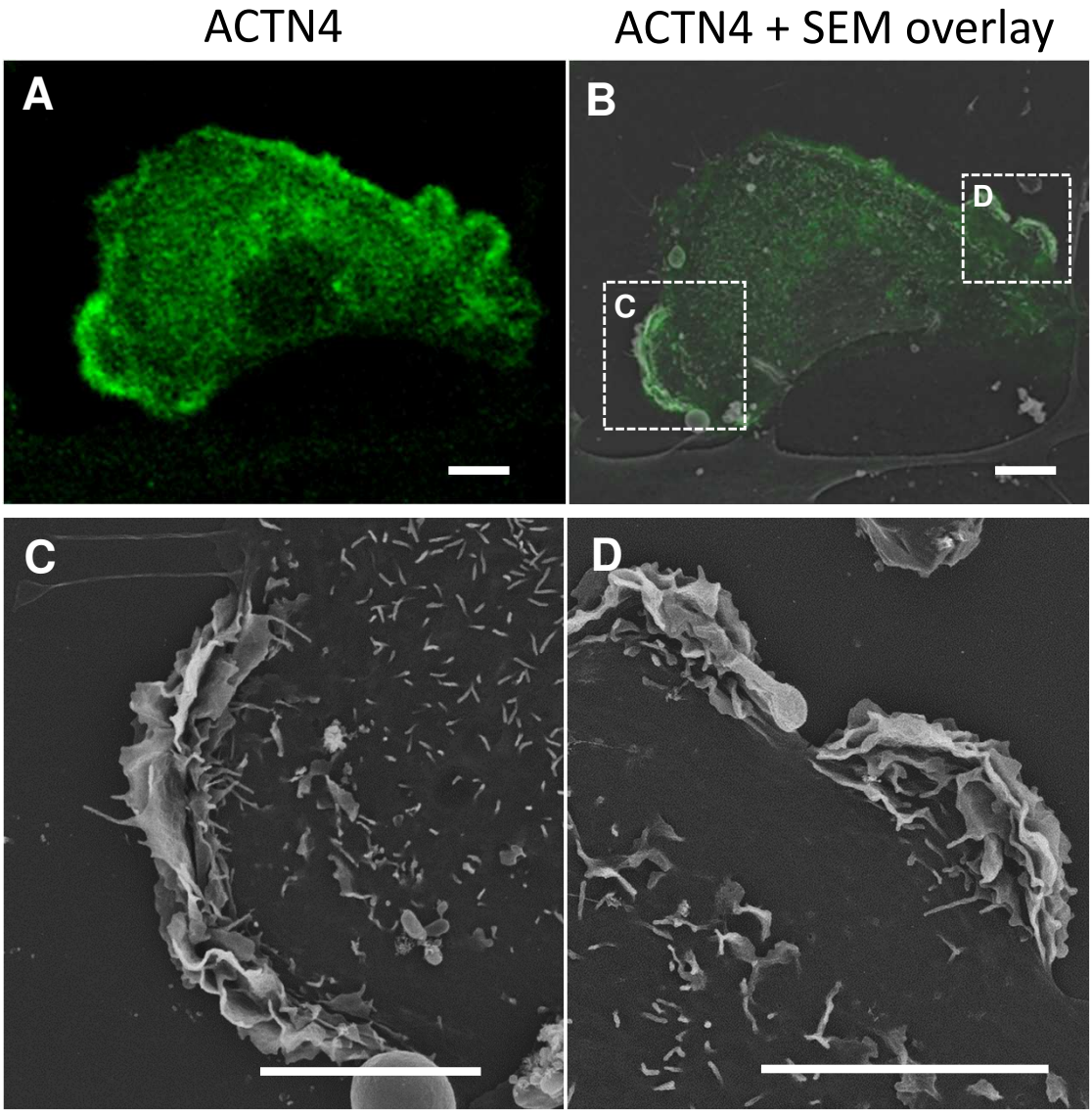

# Figure 6

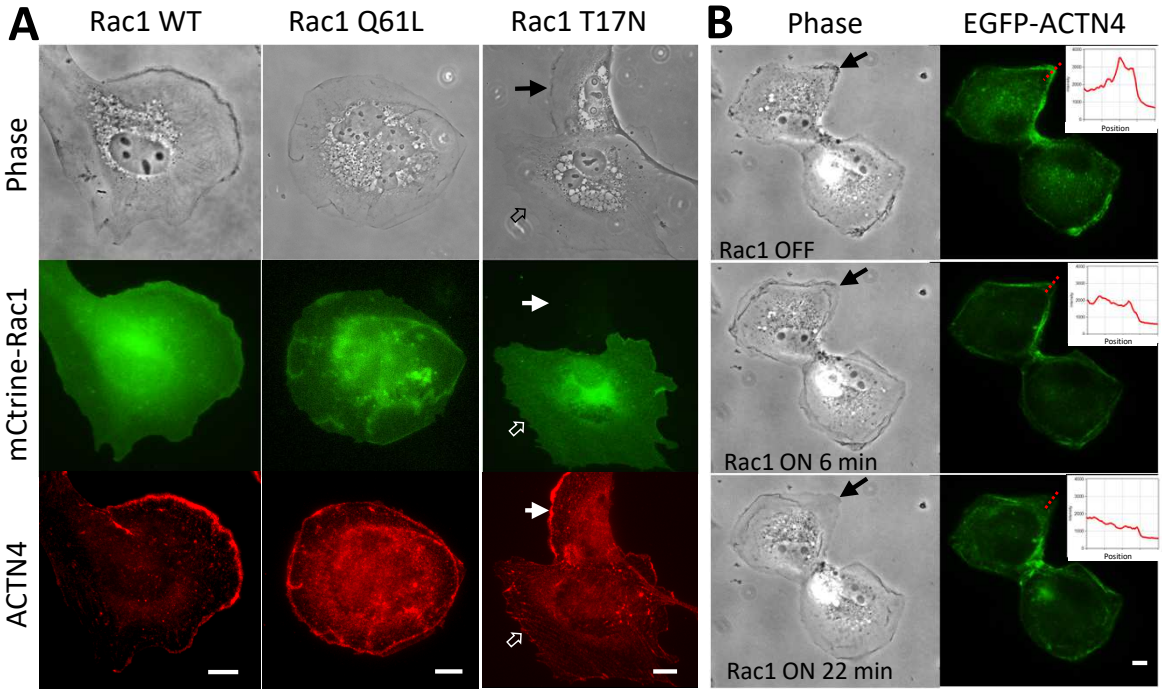
A
Rac1 WT
Rac1 Q61L
Rac1 T17N
Phase
mCtrine-Rac1
ACTN4
B
Phase
EGFP-ACTN4
Rac1 OFF
Rac1 ON 6 min
Rac1 ON 22 min

# Figure 7

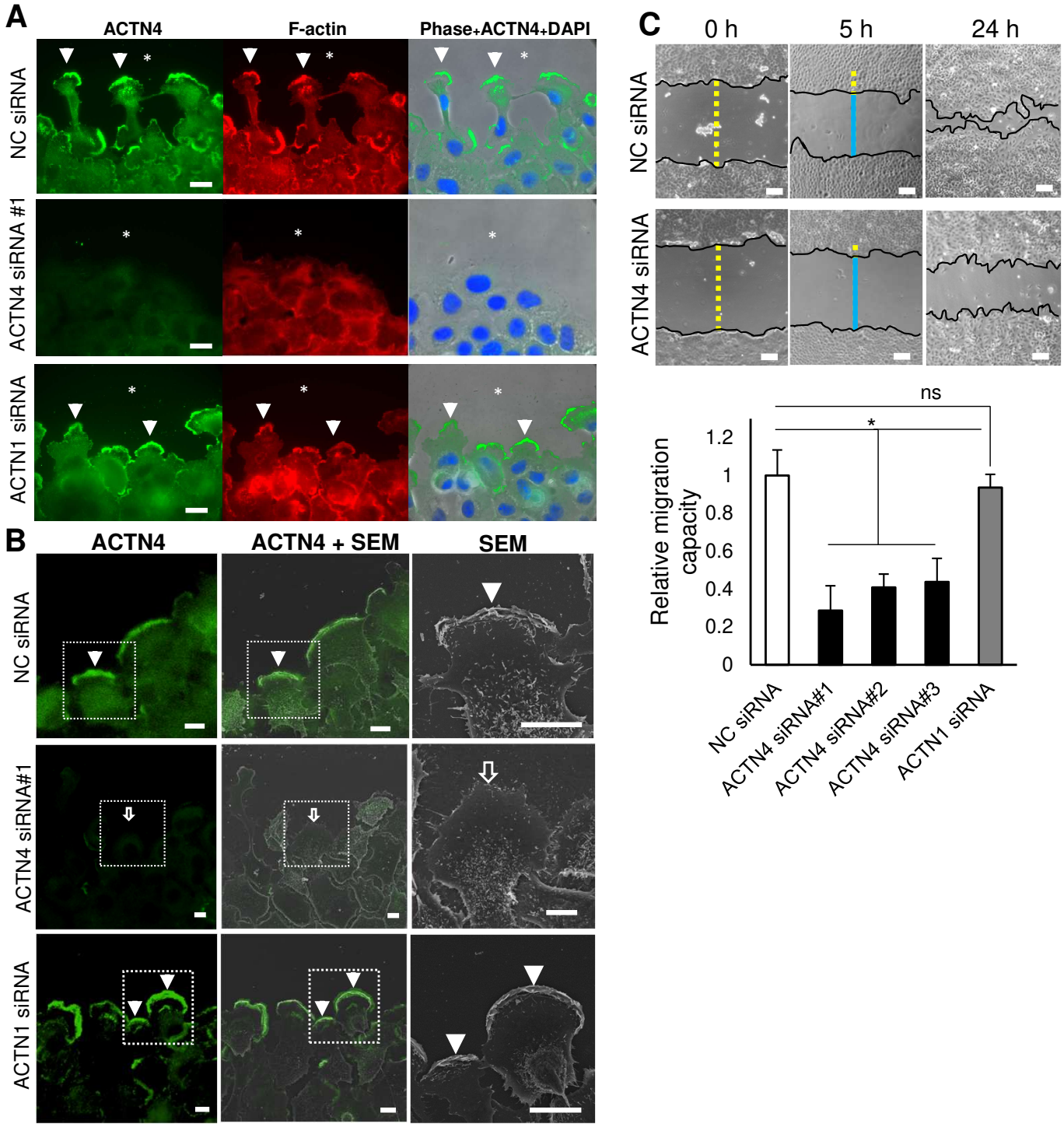
A
ACTN4
F-actin
Phase+ACTN4+DAPI
NC siRNA
ACTN4 siRNA #1
ACTN1 siRNA
B
ACTN4
ACTN4 + SEM
SEM
NC siRNA
ACTN4 siRNA#1
ACTN1 siRNA
C
0 h
5 h
24 h
NC siRNA
ACTN4 siRNA
ns
*
Relative migration capacity
1.2
1
0.8
0.6
0.4
0.2
0
NC siRNA
ACTN4 siRNA#1
ACTN4 siRNA#2
ACTN4 siRNA#3
ACTN1 siRNA

# Figure 8

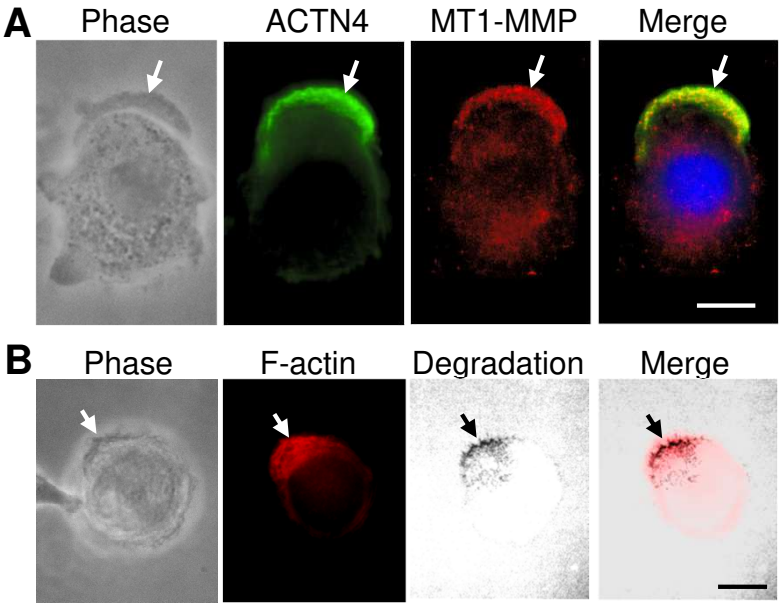
A
Phase
ACTN4
MT1-MMP
Merge
B
Phase
F-actin
Degradation
Merge

## Supplementary Figure S1

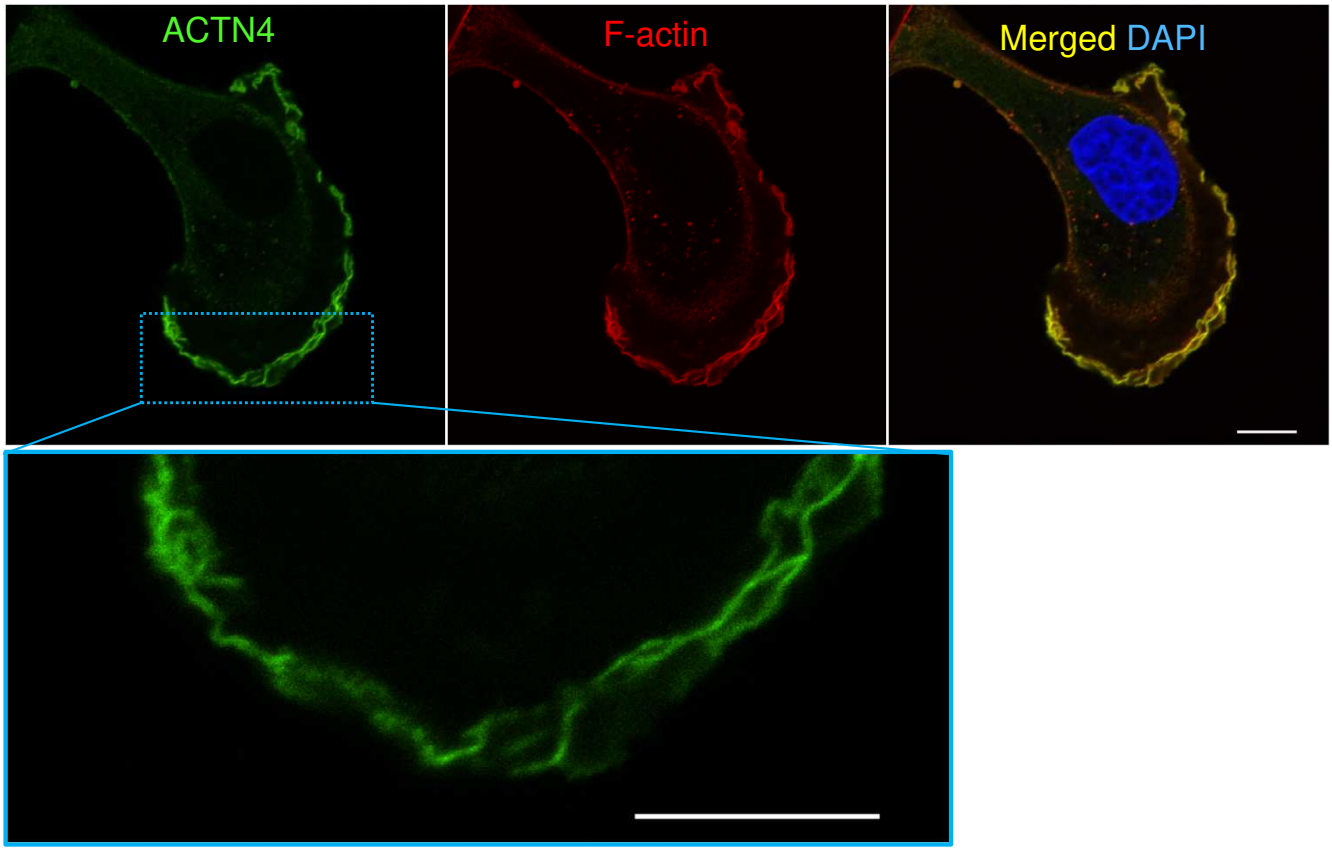


**Supplementary Figure S1. High-resolution confocal microscopy showing the representative localization of ACTN4 in L-type BSC-1 cells.** BSC-1 cells transfected with EGFP-ACTN4 were fixed with 4% PFA. F-actin was stained with Alexa Fluor 568 phalloidin. Nuclei were stained with DAPI. High-resolution images were acquired with the Nikon AX NSPARC confocal laser microscope system. ACTN4 was observed to be associated with wavy membranous structures at the leading edge of lamellipodium. Actin stress fibers were not observed in L-type cells. The blue-boxed region was enlarged in the lower frame. Scale bars: 10 μm.

## Supplementary Figure S2

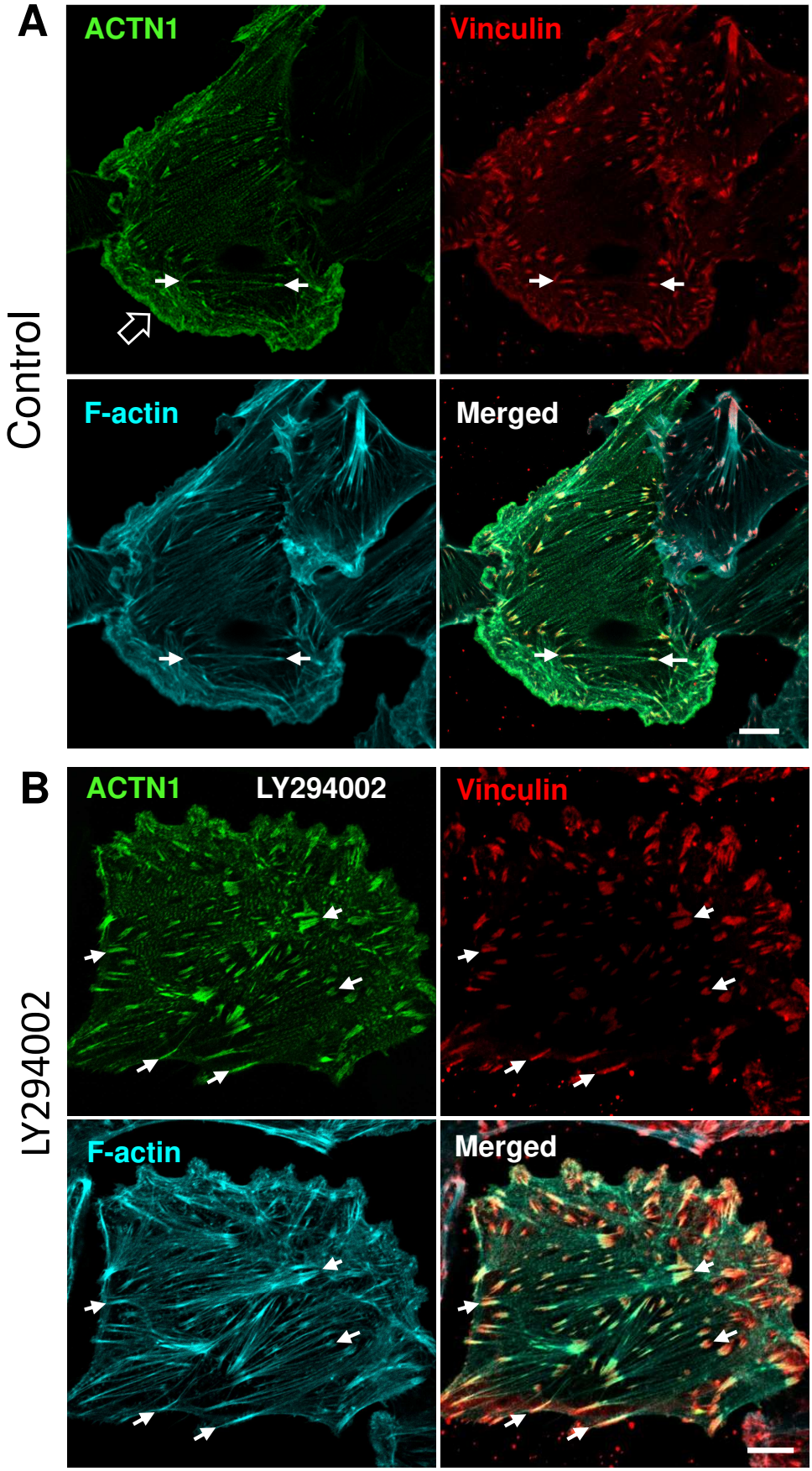


**Supplementary Figure S2. High-resolution confocal microscopy showing the representative localization of ACTN1 in control BSC-1 cells (A) and LY294002-treated cells (B).** BSC-1 cells transfected with EGFP-ACTN1 were treated with LY294002, followed by fixation with 4% PFA. Cells were immunostained with an anti-vinculin antibody, which labels focal adhesions. F-actin was stained with Acti-stain 670. Images were acquired with the Nikon AX NSPARC confocal laser microscope system. (A) ACTN1 was localized to actin stress fibers and focal adhesions (arrows) in control BSC-1 cells. Localization of ACTN1 to lamellipodia (open arrow) was modest. (B) The localizations of ACTN1 in actin stress fibers and focal adhesions (arrows) was not diminished by the LY294002 treatment. Scale bars: 10 μm.

## Supplementary Figure S3

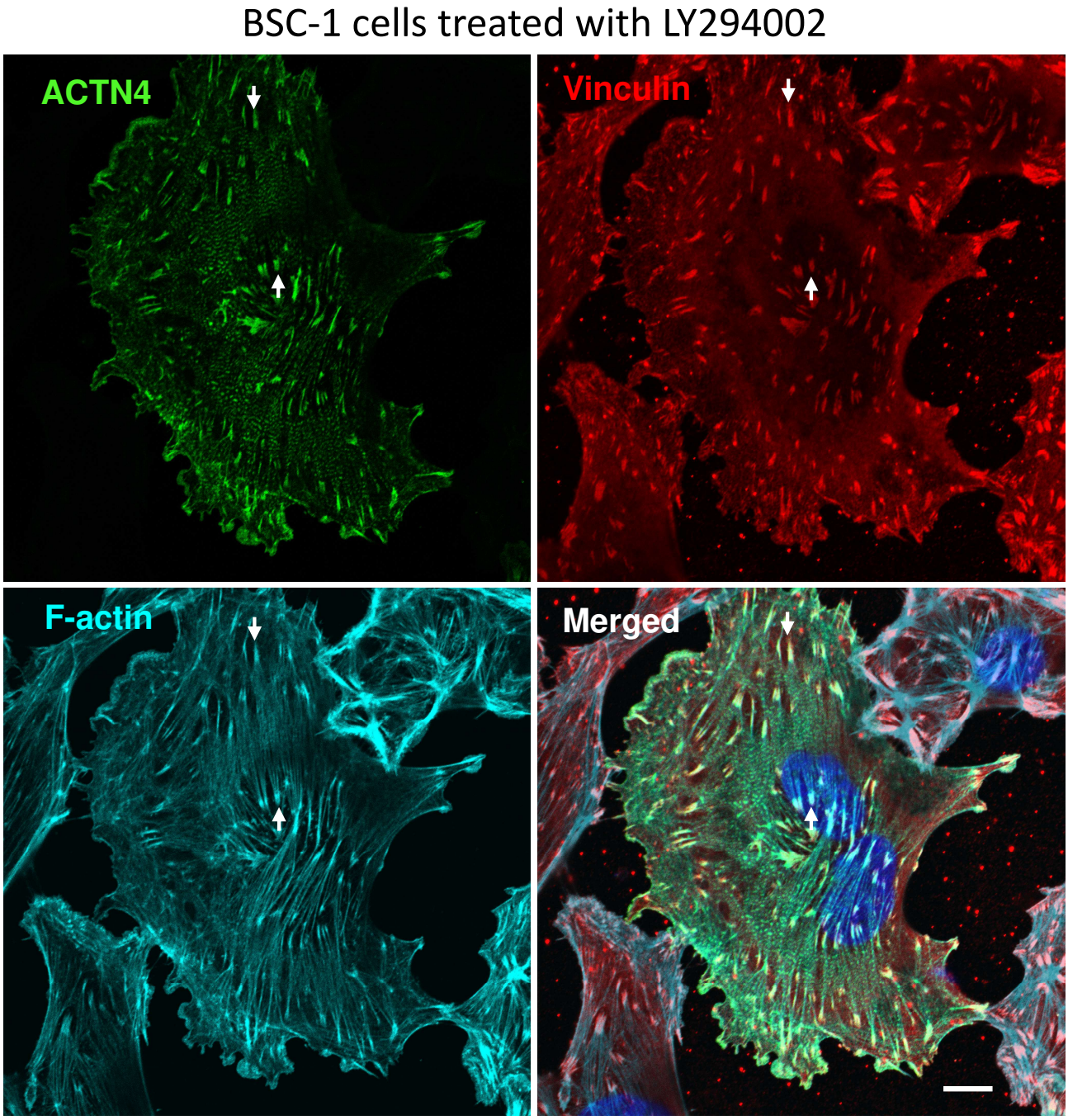


**Supplementary Figure S3. High-resolution confocal microscopy showing the representative localization of ACTN4 in LY294002-treated BSC-1 cells.** BSC-1 cells transfected with EGFP-ACTN4 were treated with 25 μM LY294002 for 30 min and fixed with 4%PFA. Cells were immunostained with an anti-vinculin antibody, which labels focal adhesions. F-actin was stained with Acti-stain 670. Images were acquired with the Nikon AX NSPARC confocal laser microscope system. After LY294002 treatment, the localization of ACTN4 in lamellipodia was markedly diminished, while ACTN4 in actin stress fibers and focal adhesions (arrows) was sustained. Scale bars: 10 μm.

## Supplementary Figure S4

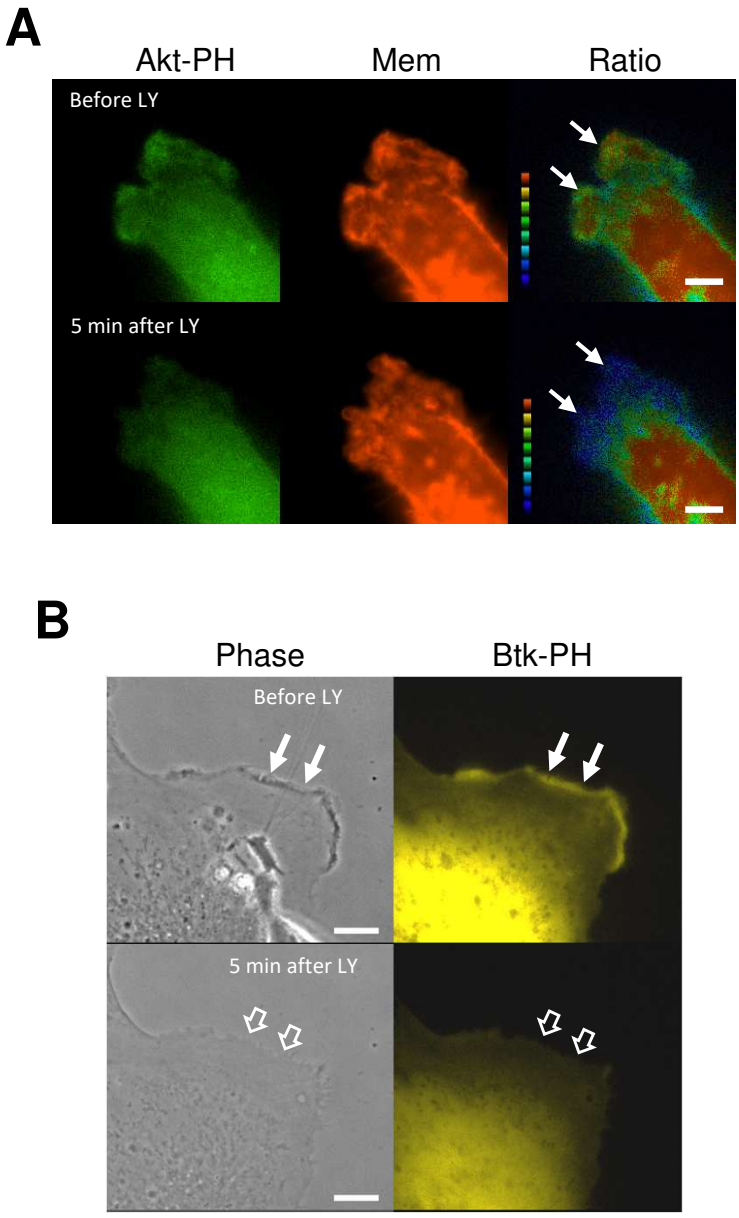


**Supplementary Figure S4. Effect of LY294002 on 3' phosphoinositide in lamellipodial leading edges.** (A) BSC-1 cells were co-transfected with mCitrine-Akt-PH and mCherry-membrane (Mem). Ratio images of Akt-PH/Mem showing that PI(3,4,5)$P_3$/PI83,4$P_2$ concentrations in the plasma membrane were created by the MetaMorph imaging system as previously described [21]. Note that PI(3,4,5)$P_3$/PI83,4$P_2$ concentrations in the membrane of lamellipodial leading edges (arrows) decreased by the addition of 25 μM LY294002 (LY). (B) Live-cell microscopy of a BSC1 cell showing the effect of LY294002 on lamellipodia enriched with PI(3,4,5)$P_3$ monitored with YFP-Btk PH domain. In BSC-1 cells expressing YFP-Btk PH domain, PI(3,4,5)$P_3$ was detected at the leading edge of lamellipodium (arrows). After the addition of LY, PI(3,4,5)$P_3$ markedly diminished in the lamellipodium. The corresponding phase-contrast images are shown in the left frame. It is also notable that the phase-dark structures at the leading edge of the lamellipodium disappeared after the addition of LY (open arrows). Scale bars: 10 μm. A corresponding movie is available in the supplementary materials (Movie 2).

## Supplementary Figure S5

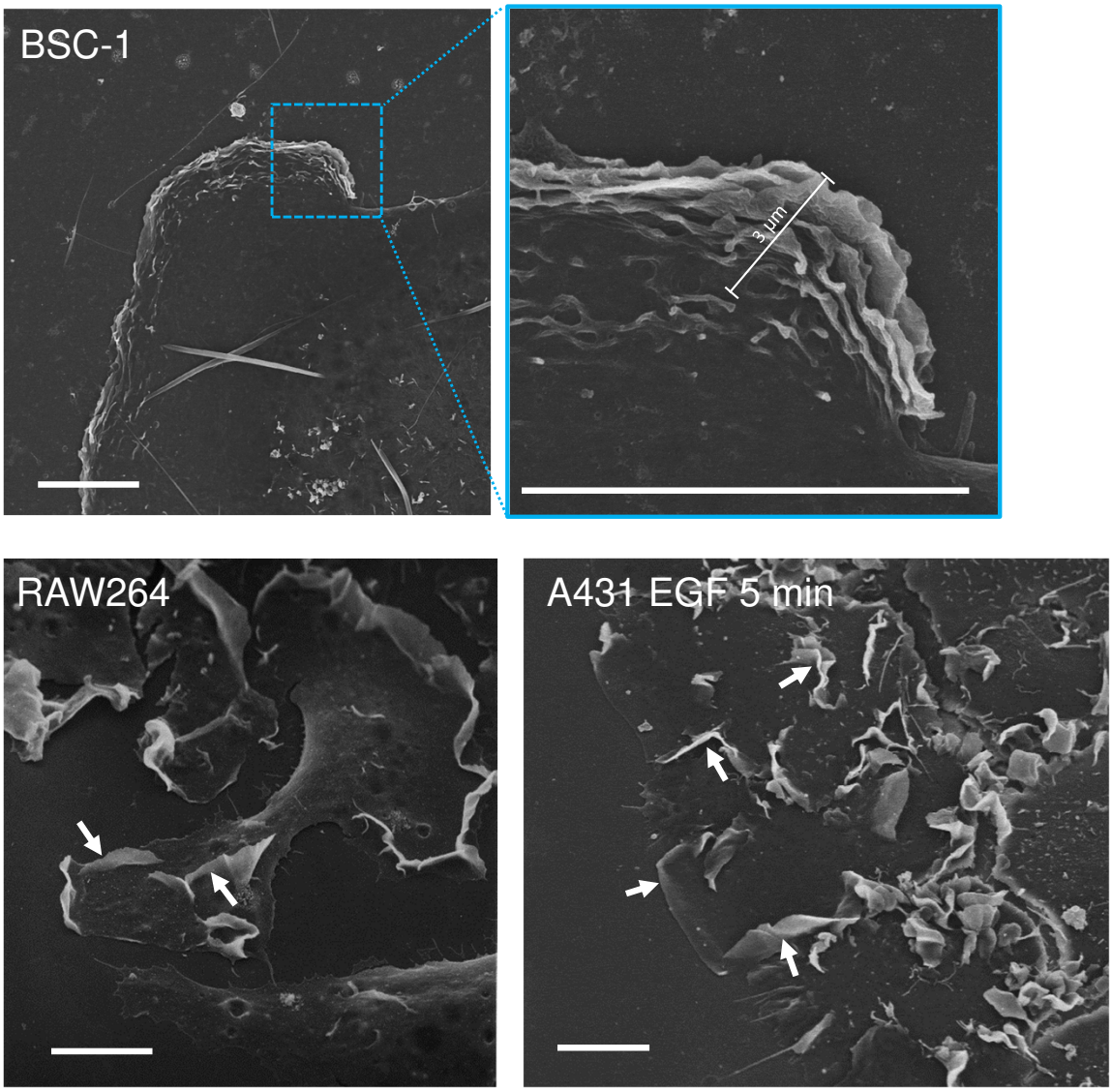


**Supplementary Figure S5. Scanning EM showing that ruffle-edge lamellipodia are distinct from membrane ruffles arising from flat lamellipodia in RAW264 macrophages and EGF-stimulated A431 cells.** Multi-layered membrane ruffles of lamellipodial leading edge in BSC-1 cells are smaller and more tightly stacked than membrane ruffles in RAW264 and EGF-stimulated A431 cells. Membrane ruffles arising from flat lamellipodia extend to the dorsal surface of RAW264 and A431 cells (arrows), whereas the presence of layered membrane ruffles is restricted to within ~3 µm from the leading edge of the lamellipodium (upper right enlarged image of the boxed area) in BSC-1 cells. Scale bars: 10 µm.

## Supplementary Figure S6

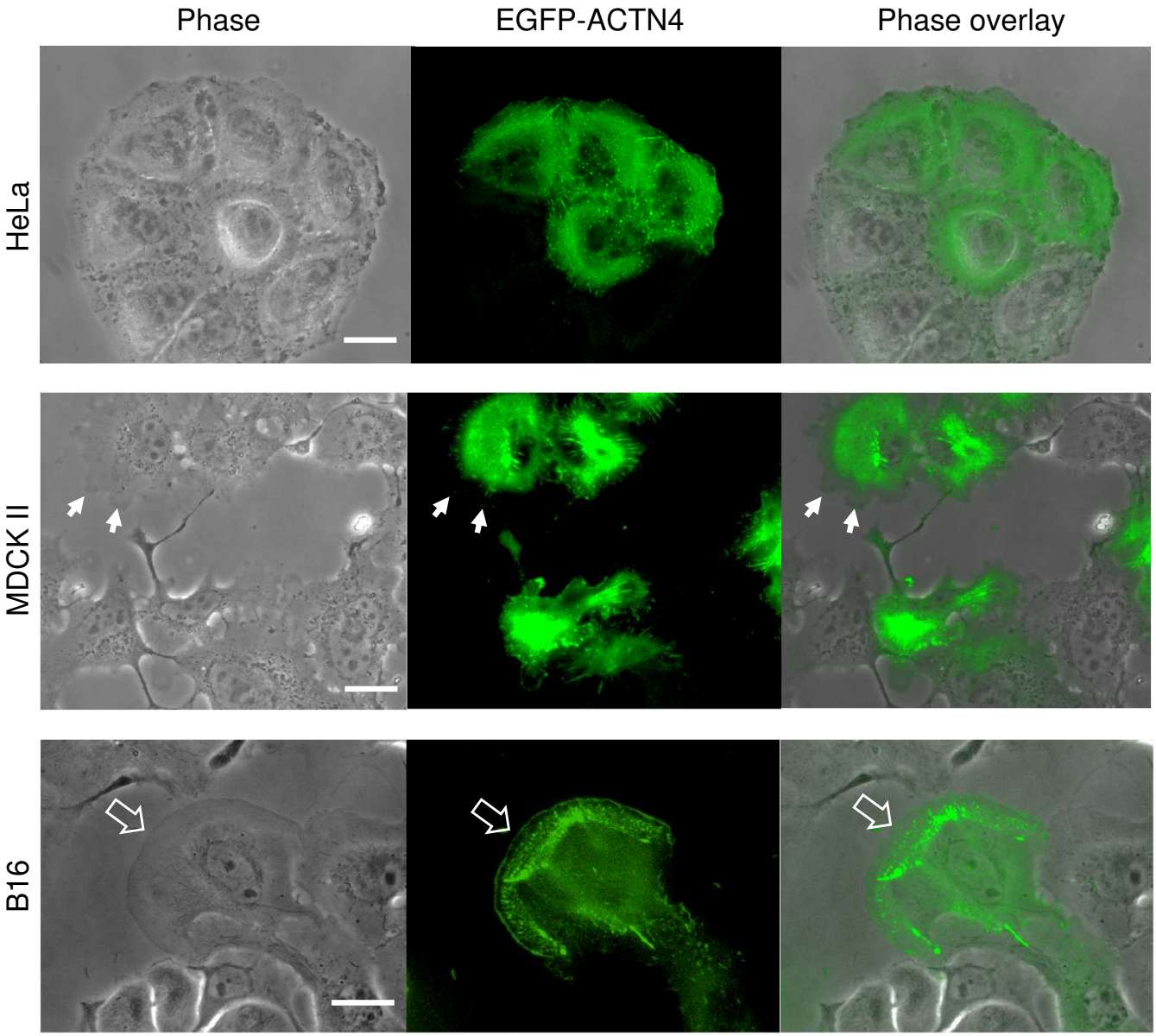


**Supplementary Figure S6. ACTN4-enriched lamellipodia were rarely observed in HeLa, MDCK II, or B16 cells.** Live cells transfected with EGFP-ACTN4 were observed by phase-contrast and fluorescence microscopy. In HeLa cells, ACTN4 was predominantly localized in stress fibers and focal contacts. Although MDCK II cells frequently showed the extension of lamellipodia (arrows), they did not have ACTN4-enriched ruffle edge. B16 cells showed well-developed lamellipodia (open arrow), but the ACTN4 localization in their flat leading edges was modest. Scale bars: 10 µm.

## Supplementary Figure S7

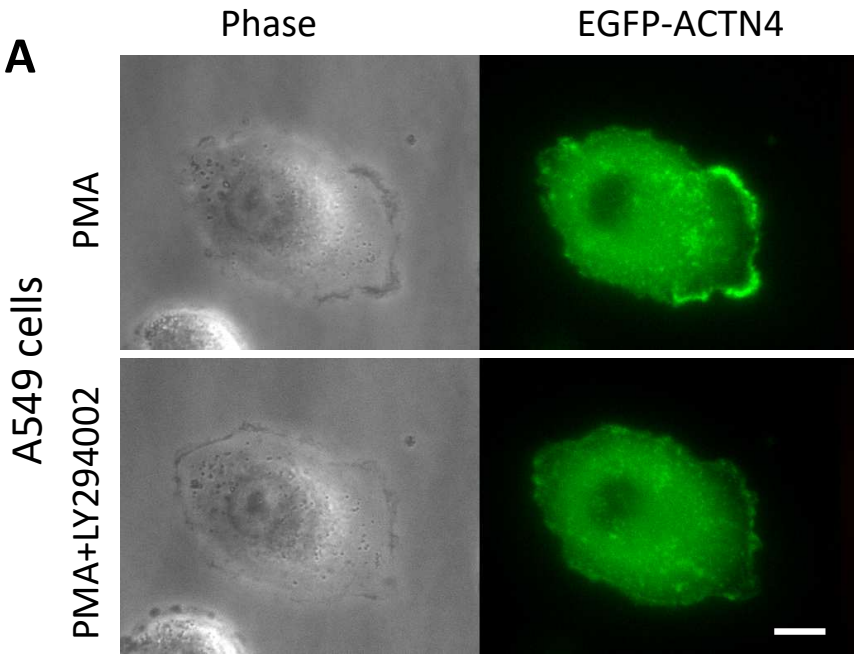


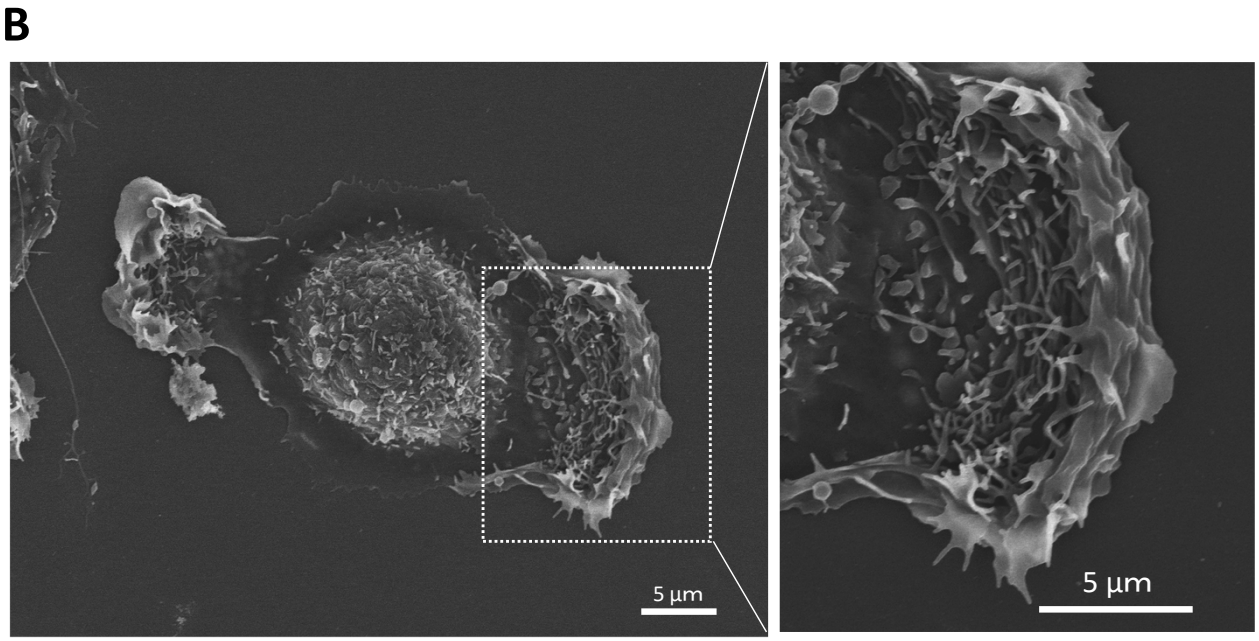


**Supplementary Figure S7. Presence of ACTN4-enriched ruffle-edge lamellipodia in A549 cells stimulated with PMA.** (A) By live-cell imaging of A549 cells transfected with EGFP-ACTN4, ACTN4-enriched lamellipodia were frequently observed in PMA-stimulated A549 cells (upper column). ACTN4-enriched lamellipodia diminished with the addition of LY294002 (lower column). Scale bar: 10 µm. (B) Scanning EM showing that lamellipodia have multilayered membrane folds at their leading edges in PMA-stimulated A549 cells. A magnified view of the boxed area is shown in the right frame. Scale bars: 5 µm.

## Supplementary Figure S8

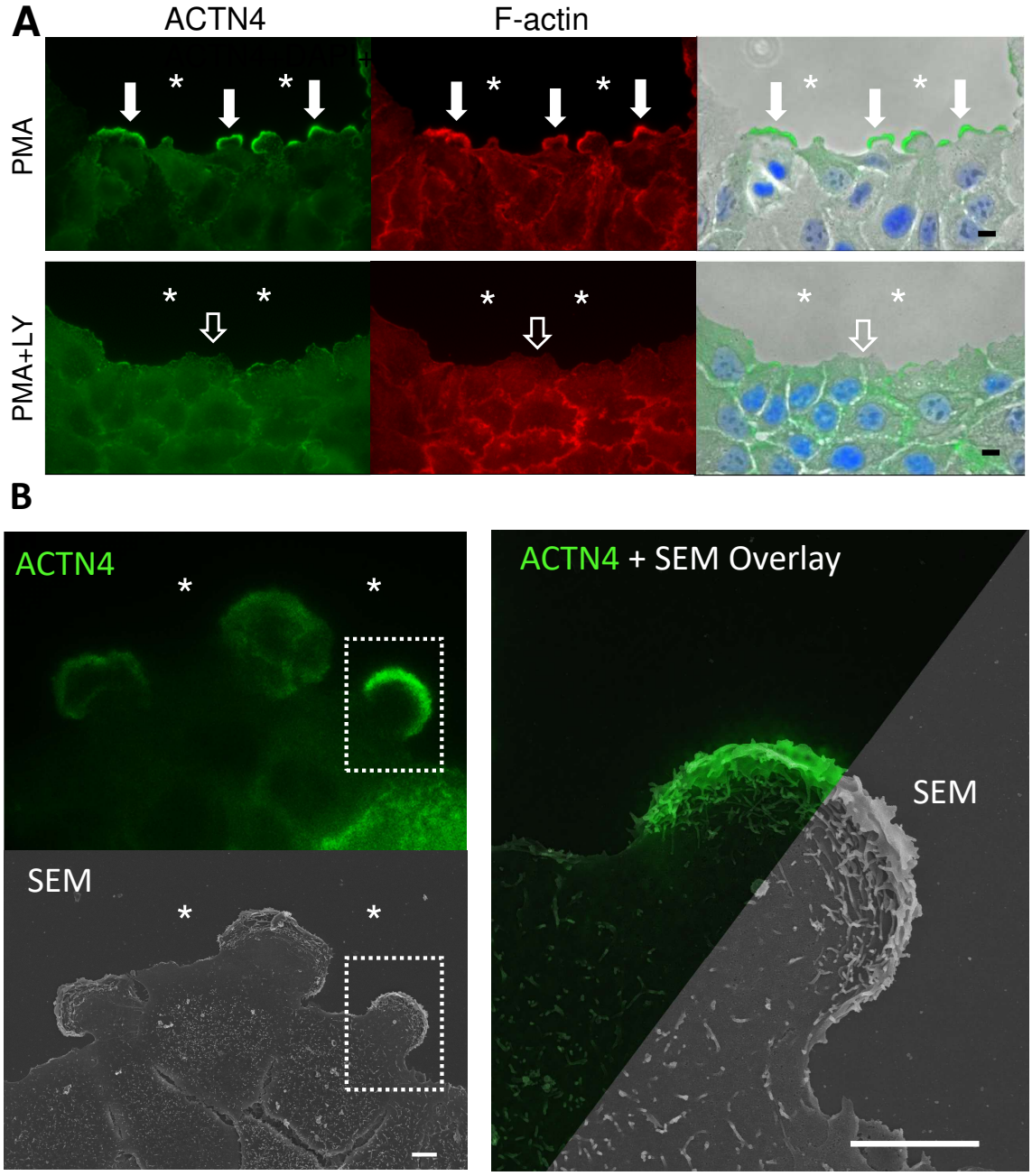


**Supplementary Fig. S8. Formation of ACTN4-enriched ruffle-edge lamellipodia during wound healing in human non-small cell lung cancer A549 cell monolayer culture.** (A) Three hours after creating a wound on the monolayer culture, the cells were fixed with PFA. Endogenous ACTN4 was immunostained with an anti-ACTN4 antibody, followed by Alexa Fluor 488-labeled secondary antibody (green). F-actin was stained with Alexa Fluor 568-phalloidin (red). Nuclei were stained with DAPI (blue). In phorbol 12-myristate 13-acetate (PMA)-stimulated A549 cells, ACTN4-enriched lamellipodia (arrows) were formed in migrating cells toward the wounded space (asterisks). The formation of ACTN4-enriched lamellipodia was inhibited by LY294002 (LY) treatment (open arrows). (B) CLEM reveals that ACTN4-enriched lamellipodia protruding toward the wounded space (asterisks) have multilayered membrane folds at their leading edges. A magnified view of the boxed area is shown in the right frame. Scale bars: 10 μm.

## Supplementary Figure S9

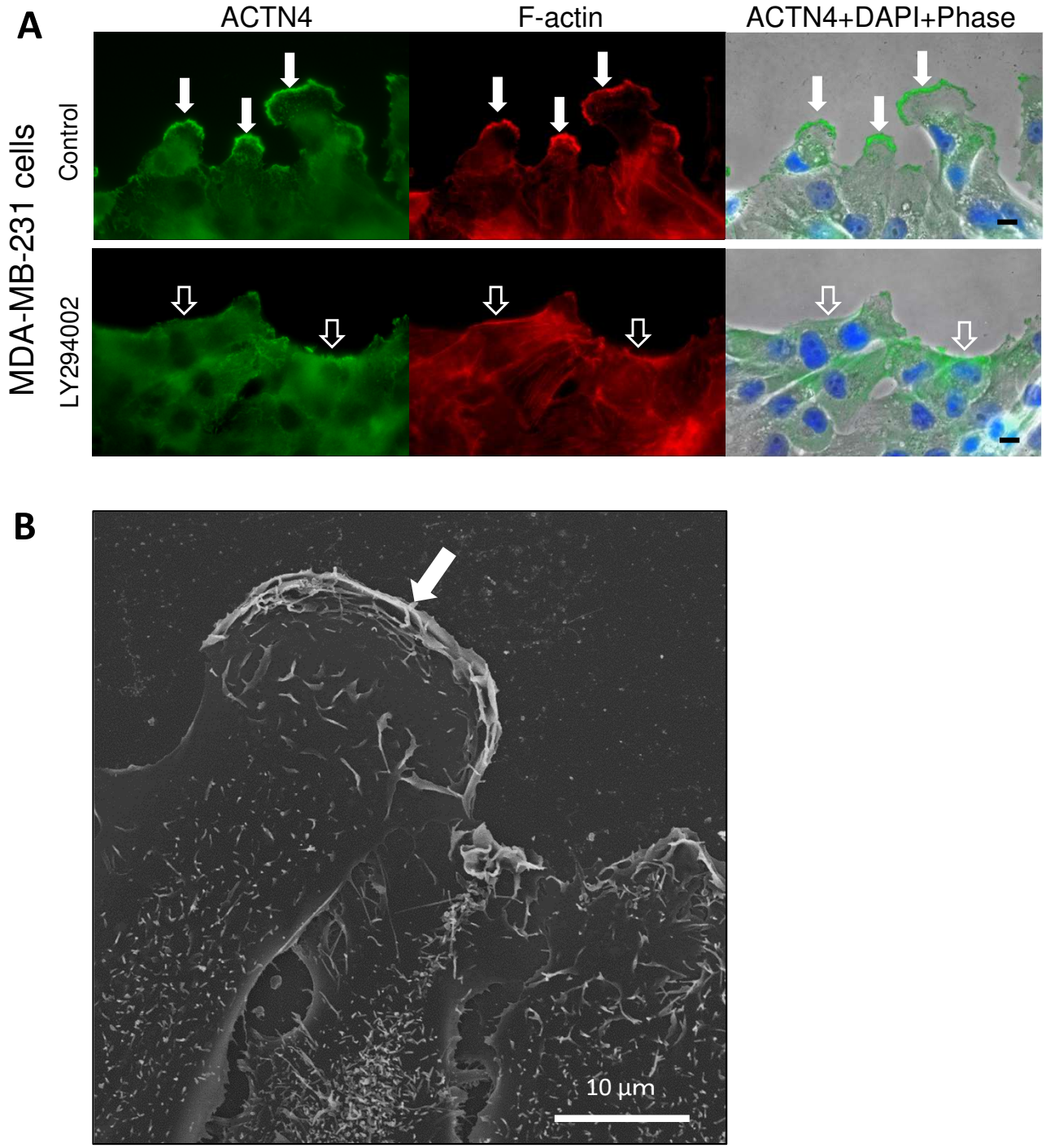


**Supplementary Figure S9. Formation of ACTN4-enriched ruffle-edge lamellipodia during wound healing of human invasive breast cancer MDA-MB-231 cell monolayer culture.** (A) Three hours after creating a wound on the monolayer culture, cells were fixed and stained with anti-ACTN4 (green) and Alexa Fluor 564-phalloidine (red). In control MDA-MB-231 cells, ACTN4-enriced lamellipodia were formed in migrating cells toward the wounded space (arrows). ACTN4-enriched lamellipodia were not observed after LY294002 treatment (open arrows). Scale bars: 10 µm. (B) Scanning EM reveals that lamellipodia extending toward the wounded space have multilayered membrane folds (arrow). Scale bars: 10 µm.

## Supplementary Figure S10

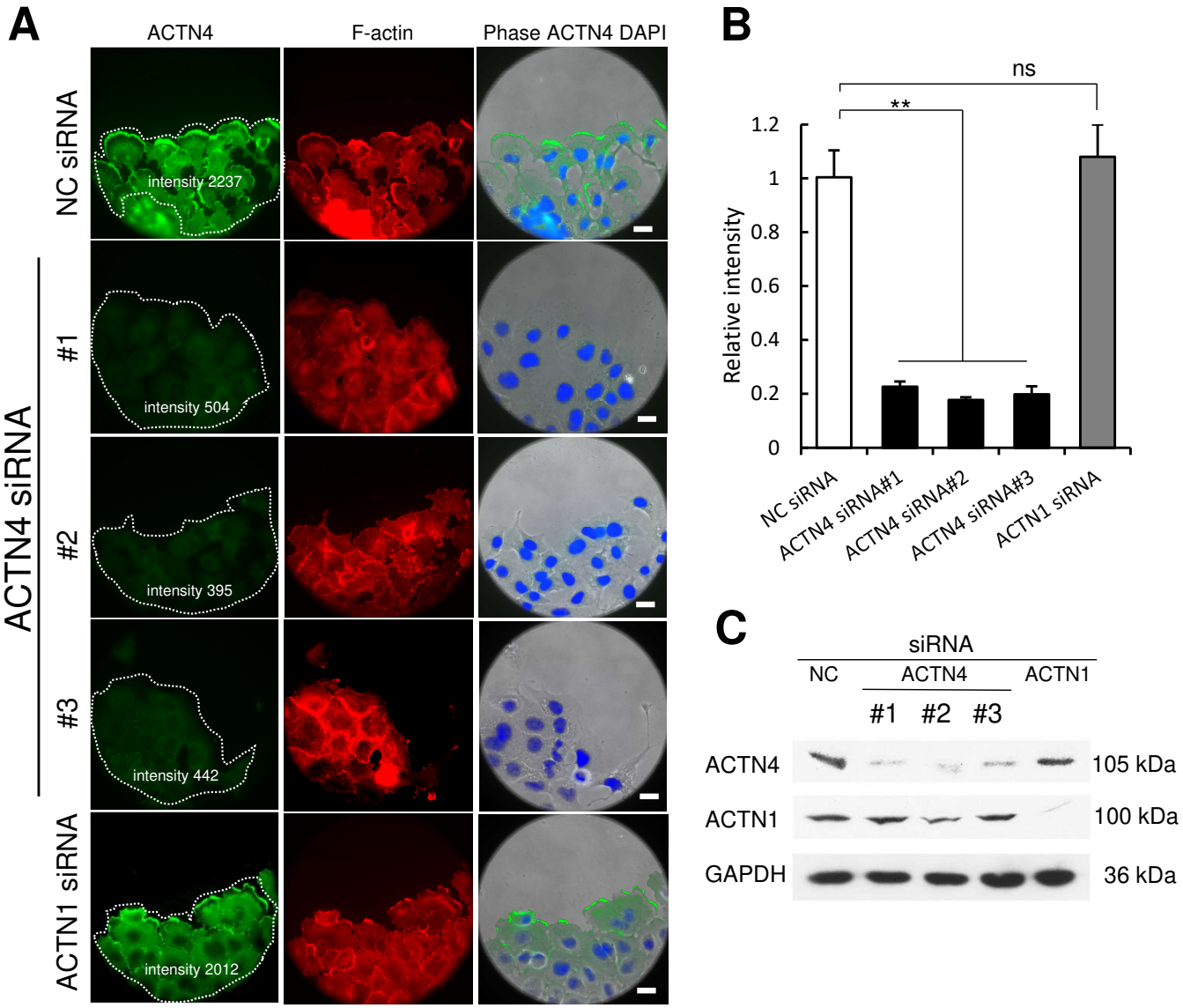


**Supplementary Figure S10. Isoform-specific knockdown of ACTN4 by siRNA.** (A) A549 cells subconfluently cultured on coverslips were transfected with negative control (NC) siRNA, three ACTN4 siRNAs (#1, #2, #3), or ACTN1 siRNA. Five hours after scratching the monolayer of culture cells, the cells were fixed and subjected to ACTN4 immunocytochemistry and F-actin staining. Nuclei were stained with DAPI. Scale bars: 20 μm. (B) Expression levels of ACTN4 were quantified using immunofluorescence intensities measured by the MetaMorph imaging software. The average fluorescence intensity values in >8 cell areas facing the wounded space in each coverslip were calculated. ACTN4 fluorescence intensity was normalized to the intensity of NC siRNA-transfected cells after background correction. ACTN4 siRNA (#1-3), but not ACTN1 siRNA, significantly reduced ACTN4 protein expression (**$p<0.01$, n=3). Values are expressed as the means ± SEM of triplicate experiments and are representative of two other independent experiments. The fluorescent intensity in representative images was shown in the cell area (dotted line in A). (C) Immunoblot analysis with anti-ACTN4 or anti-ACTN1 antibodies demonstrated that ACTN4 siRNAs #1-3 reduce ACTN4 protein levels, but not ACTN1 protein levels. Immunoblotting with an anti-GAPDH antibody verified equal amounts of total protein loading.